NASA Technical Memorandum 103204

Elastic/Plastic Analyses of Advanced Composites Investigating the Use of the Compliant Layer Concept in Reducing Residual Stresses Resulting from Processing

Steven M. Arnold
Lewis Research Center
Cleveland, Ohio

Vinod K. Arya
University of Toledo
Toledo, Ohio

and

Matthew E. Melis
Lewis Research Center
Cleveland, Ohio

September 1990

NASA

ELASTIC/PLASTIC ANALYSES OF ADVANCED COMPOSITES INVESTIGATING THE USE OF THE COMPLIANT LAYER CONCEPT IN REDUCING RESIDUAL STRESSES RESULTING FROM PROCESSING

Steven M. Arnold
National Aeronautics and Space Administration
Lewis Research Center
Cleveland, Ohio

and

Vinod K. Arya*
University of Toledo
Toledo, Ohio

and

Matthew E. Melis
National Aeronautics and Space Administration
Lewis Research Center
Cleveland, Ohio

SUMMARY

High residual stresses within metal and intermetallic matrix composite systems can develop upon cooling from the processing temperature to room temperature due to the coefficient of thermal expansion (CTE) mismatch between the fiber and matrix. As a result, within certain composite systems, radial, circumferential, and/or longitudinal cracks have been observed to form at the fiber–matrix interface region. The compliant layer concept (insertion of a compensating interface material between the fiber and matrix) has been proposed to reduce or eliminate the residual stress buildup during cooling and thus minimize cracking. The present study investigates both elastically and elastic–plastically the viability of the proposed compliant layer concept.

A detailed parametric study was conducted utilizing a unit cell model consisting of three concentric cylinders to determine the required character (i.e., thickness and mechanical properties) of the compliant layer as well as its applicability. The unknown compliant layer mechanical properties were expressed as ratios of the corresponding temperature dependent Ti–24Al–11Nb (a/o) matrix properties. The fiber properties taken were those corresponding to SCS–6 (SiC). Results indicate that the compliant layer can be used to reduce, if not eliminate, radial and circumferential residual stresses within the fiber and matrix and therefore also reduce or eliminate the radial cracking. However, with this decrease in in–plane stresses, one obtains an increase in longitudinal stress, thus potentially initiating longitudinal cracking. Guidelines are given for the selection of a specific compliant material, given a perfectly bonded system.

INTRODUCTION

Metal and intermetallic matrix composites are currently being considered for advanced aerospace applications due to their attractive high strength–to–density ratio. However, due to the inherent coefficient of thermal expansion (CTE) mismatch between

*National Research Council - NASA Research Associate.

fiber and matrix, upon cooling, high residual stresses exist in these composite systems from the processing consolidation temperature to room temperature. These residual stresses may be large enough in magnitude to generate radial, circumferential (interfacial debonding), and/or longitudinal cracks within the matrix. For example, in the case of SiC/Ti_3Al+Nb (or alternately Ti–24Al–11Nb (a/o)) and SiC/Ti–15–3 systems, microscopic radial cracks have been observed to be present at the fiber–matrix interface after fabrication and to proliferate after thermal cycling (ref. 1). Figure 1 shows radial cracking at the fiber/matrix interface, both after fabrication and after 1000 thermal cycles, for the SiC/Ti_3Al+Nb system of interest in this study. In addition to radial cracks, other, less frequently observed, crack orientations are illustrated schematically in figure 2(a)[1].

A number of potential solutions for reducing the residual stress field have been proposed recently. Examples of some potential solutions are high CTE fibers, fiber preheating, and the compliant layer concept. The compliant layer concept (the subject of the present study) entails the insertion, or addition, of an interface material between the fiber and matrix to reduce or eliminate the residual stress field, and therefore the initiation of cracks, developed during cooldown. Of particular interest is the reduction in the tensile hoop stress σ_θ (fig. 2(b)) within the matrix, which is the cause of the predominantly observed radial cracking (figs. 1 and 2(a)).

Previous investigations have been undertaken to examine the sign and magnitude of the resulting residual stress field (refs. 2 to 4) within a composite system as well as the effect of including a compliant layer (refs. 5 to 7). Varying degrees of simplification and idealization have been adopted, the most common being the assumption of linear elasticity with regard to the behavior of the matrix material. In the present study, a variety of assumptions with regard to boundary conditions and material behavior are examined within the context of a unit cell composed of three concentric cylinders (see fig. 2(b)). Here, each cylinder is associated with a different homogeneous isotropic material; that is, fiber, compliant layer, and matrix, that may be thermoelastic and/or plastic. The stress analysis is a three–dimensional study (assuming perfect bonding between cylinders) and considers only the residual stresses due to the initial cooldown cycle during fabrication.

The objective of this report is to define the required character (i.e., thickness and mechanical properties) of a compliant, or compensating, layer which will minimize the local

[1]For readers familiar with ASTM E 616–89 standard terminology relating to fracture testing, the designation for a radial, circumferential, or longitudinal crack as reported here, can alternatively be denoted as (C–R or C–L), (R–C or R–L), or (L–C or L–R), depending upon the direction of the crack propagation.

tensile residual stresses within the system and thereby reduce the tendency toward cracking. The analysis is both analytical and numerical (finite element method) and is divided into two parts. The first part contains results associated with a linear elastic and thermoelastic stress analysis and parametric study, in which a variety of simplifying assumptions are assessed. The second part contains results associated with a thermoelastic–plastic finite element stress analysis and parametric study. A section is then devoted to identifying candidate compliant layer materials. Finally, the report concludes with a discussion of current issues and future work, followed by a summary of main conclusions.

LINEAR ELASTIC STRESS ANALYSIS

The present investigation begins by revisiting the solution of a linear elastic temperature–independent concentric cylinder model both analytically and numerically. The motivation behind this starting point is twofold. The first is to obtain an analytical solution to study the problem and verify the accuracy (mesh density) of the finite element idealization employed; the second is to assess the significance of various assumptions imposed by ourselves as well as by previous investigators (refs. 2, 3 and 5); for example, boundary conditions, decoupling of in–plane and longitudinal stresses, and temperature–independent versus dependent material properties.

Description of the Analytical Concentric Cylinder Model

Consider a composite cylinder model, consisting of a single fiber (of radius a) embedded in coaxial cylindrical shells of an interface material (outer radius b) and matrix material with outer radius c, as shown in figure 2(b). Owing to the obvious cylindrical symmetry, we treat the problem in cylindrical polar coordinates r,θ and z. Assuming the application of a uniform temperature change from a processing consolidation temperature to room temperature ($\Delta T = -1425^{o}F$) and planes remaining plane in the z direction, it follows from symmetry that the stresses ($\sigma_r,\sigma_\theta,\sigma_z$) and strains ($e_r,e_\theta,e_z$) are independent of the angle (θ) and are functions only of r. Similarly, we assume that each cylinder is composed of a homogeneous isotropic material and that a perfect bond between fiber, interface, and matrix exists.

Given these assumptions, the following linear thermoelastic stress–strain relations can be written for each cylinder.

$$\sigma_r = \frac{E}{(1-2\nu)(1+\nu)}\{(1-\nu)e_r + \nu(e_\theta+e_z) - (1+\nu)\alpha T\}$$

$$\sigma_\theta = \frac{E}{(1-2\nu)(1+\nu)}\{(1-\nu)e_\theta + \nu(e_r+e_z) - (1+\nu)\alpha T\} \quad (1)$$

$$\sigma_z = \nu(\sigma_r+\sigma_\theta) + E(e_z - \alpha T)$$

where σ is the Cauchy stress, e is the total strain, ν is the Poisson ratio, E is Young's Modulus, α is the coefficient of thermal expansion for the associated material, and T is the change in temperature (i.e., $T = T_c - T_o$ where T_c is the current applied temperature and T_o is the reference temperature).

Similarly, taking into account symmetry, the required equations of equilibrium which the stresses must satisfy are

$$\frac{d}{dr}(\sigma_r) + \frac{1}{r}(\sigma_r - \sigma_\theta) = 0 \quad (2)$$

and equilibrium in the z direction for the entire system is

$$\int_{r=0}^{r=c} \sigma_z \pi r dr = 0 \quad (3)$$

while compatibility requires that

$$e_r = \frac{d}{dr}(re_\theta) \quad (4)$$

where the strain–displacement relations are

$$e_r = \frac{d}{dr}(u(r))$$

$$e_\theta = \frac{u(r)}{r} \quad (5)$$

and we assume planes remain plane; that is,

$$e_z = \text{constant} \quad (6)$$

Note that u(r) is the radial displacement field.

Upon substitution of equations (1),(2), and (4) to (6), one may obtain expressions for the radial displacement and stress components for a generalized plane strain circular cylinder (see appendix A). Given these expressions that are valid for a single circular cylinder, a variety of laminated concentric cylinder models can be formulated by merely applying the appropriate boundary conditions (see table I) and equation (3).

End and Surface Boundary Conditions

Figure 3 illustrates schematically the two types of end and surface boundary conditions considered in this study; that is, plane strain (e_z=0) and generalized plane strain ($e_z \neq 0$) end constraints and a free surface constraint on the unit cell versus a free surface on a homogenized outer cylinder surrounding the unit cell. The rationale behind selecting the free surface constraint stems from the thermal nature of the problem, in that all the material surrounding the unit cell is undergoing similar thermal strains. The most realistic of the two surface constraints is the case when the unit cell is surrounded by an effective, homogenized, transversely isotropic, outer cylinder (with a radius sufficiently large relative to that of the unit cell), as the influence of neighboring fibers are incorporated into the analysis through the rule of mixtures (ref. 8). Results indicate, however, that the additional complexity in this idealization is unwarranted since the residual stress field developed in the free surface case is sufficiently close to that obtained by using the homogenized outer cylinder. This is clearly shown in table II where results are given comparing the effect of surface and end boundary conditions as well as a unit cell with and without a compliant layer. The geometry (i.e., the radii a, b, and c, representing a composite with a 40 percent fiber volume ratio (a^2/b^2) and 10 percent thick (t/a) compliant layer, when applicable) and elastic (temperature–independent) mechanical material properties for this example are given in table III.

From an examination of table II, a number of conclusions can be drawn:

(a) The in–plane stress states (σ_r and σ_θ) are basically unaffected by modification of the end condition (i.e., $e_z = 0$ or e_z = constant) while the longitudinal stress (σ_z) is highly affected. In particular, the fiber stress becomes compressive under the generalized plane strain condition, while under the plane strain condition it is tensile.

(b) For a given end condition, modification of the surface constraint results in approximately a 13 percent increase in σ_r, a 5 to 10 percent decrease in σ_θ, and a 20 to 25 percent decrease in σ_z within the compliant and matrix material.

(c) Inclusion of a compliant layer material reduces the tensile hoop stress within the matrix (r=b) by approximately 25 percent while a significant stress state is produced in the compliant layer.

Because of the results shown in table II and other results not included here, the generalized plane strain end and free surface boundary conditions are assumed when conducting the following parametric studies.

Decoupling of In–plane and Longitudinal Stress Components

Turning our attention to the results of a previous investigation (ref. 5) wherein the in–plane stresses (σ_r and σ_θ) were assumed to be decoupled from the longitudinal stress, the significance of such an assumption can now be examined, since in the present analysis no assumption is made with regard to decoupling. Assuming the geometry and material properties to be those taken by Ghosn and Lerch (ref. 5), three concentric unit cell calculations have been revisited. The results are tabulated in table IV.

Upon examining table IV, it is clear that two general observations can be made. The first is that the discrepancies in the in–plane stresses (σ_r and σ_θ) are less than those in the longitudinal component (σ_z), and secondly, these discrepancies increase as the thickness of the compliant layer is increased. Furthermore, if one considers the reduction in hoop stress due to the addition of a compliant layer, one sees approximately twice the reduction for the cases in which the decoupling assumption is enforced compared with the more accurate three–dimensional analysis presented here. Therefore, the impact of this decoupling assumption on the resulting stress state is significant and detrimental (nonconservative), while its influence on the tractability of the solution is minimal. As an aside, a comparison between the effective longitudinal strain that is found by using the rule of mixture; that is,

$$e_z = \alpha_l \Delta T$$

where $$\alpha_l = \left[\frac{V_f \alpha_f E_f + V_c \alpha_c E_c + V_m \alpha_m E_m}{V_f E_f + V_c E_c + V_m E_m} \right]$$

and that calculated directly from the present analysis (e_z) is included (see table IV) and is found to be less than one percent.

Description of Finite Element Concentric Cylinder Model

Four concentric cylinder unit cell models have been idealized utilizing PATRAN (ref. 9), each with a different compliant layer thickness; that is, t/a= 0.05, 0.075, 0.1 and 0.2. Two of these mesh discretizations, those corresponding to t/a = 0.05 and 0.1, are illustrated in figures 4 and 5. The element employed is an 8–node isoparametric solid brick element with three degrees of freedom per node. A three–dimensional finite element analysis, with quarter symmetry[2] was performed using the finite element program MARC (ref. 10). The end and surface boundary conditions assumed were those of generalized plane strain and free, respectively, as discussed previously. Due to the symmetry of the problem, the natural coordinate system of choice is that of polar coordinates; therefore, transformation of the resulting stress and strain fields from the assumed (prescribed) global cartesian coordinate system of MARC is required. The resulting principle stress and strain components are then processed further by calculating the arithmetic mean between two integration points within a given element (see fig. 6). Note that an eight–point Gauss quadrature numerical integration scheme was selected that yielded four data points of interest per element, two within a given z plane.

A mesh density study was conducted to verify the accuracy of the results. The final mesh discretizations employed are those shown in figures 4 and 5. An illustration of the discretization accuracy (less than one percent in error when compared with the exact solution) is shown in figures 7, 8, and 9 in which the radial, circumferential, and longitudinal stresses are displayed as a function of radius for the case described in table III and idealized in figure 5.

Temperature–Independent Versus Dependent Material Parameters

Previously, only temperature–independent material properties have been considered for each constituent. Experiments indicate, however, that the material properties are in fact temperature–dependent, that is to say, the stiffness and CTE of the matrix and the CTE of the fiber vary with temperature. Table V summarizes the temperature–dependent behavior of the Ti_3Al+Nb matrix (elastic and plastic properties) and that of the SiC fiber (elastic only). These material data were obtained through private communications with Brindley (ref. 11) and Textron Inc (ref. 12). In order to assess the importance (with regard to modifying the resulting unit cell stress distribution) of incorporating temperature–

[2]The current problem actually possesses full rotational symmetry (i.e., is independent of the angle θ), thereby allowing the alternative use of axisymmetric elements.

dependent material behavior in the analysis, the problem with parameters given in table III was reanalyzed assuming both temperature–independent and dependent material properties. Note, as before, that the compliant layer properties are taken relative to those of the matrix for all temperatures.

Table VI contains the results of the analysis. As indicated, the difference between the temperature–dependent and independent results is approximately 11 percent. However, this difference would increase as the temperature dependence of the material properties increased. This can be illustrated theoretically by writing the incremental stress–strain relations (see appendix B). On looking ahead to conducting an elastic–plastic analysis, it is clear from Table V that the plastic material properties are highly temperature dependent. Therefore, material temperature dependence has been included in all remaining analysis results.

Compliant Layer Thermo–Elastic Parametric Study

Thus far only an assessment and validation of fundamental solution assumptions have been examined. The questions remain as to the impact of the so–called compliant layer on reducing the overall residual stress field within a composite system and as to its required character (i.e., thickness and mechanical properties).

Interpretation of Problem

Let us begin by considering, generically, the interaction of the fiber and matrix in the r–θ plane (see fig. 10(a)) and let us assume, as is the case for the present system of interest (i.e., SiC/Ti_3Al+Nb) that the CTE of the matrix is greater than that of the fiber. In this figure, a free body diagram is shown in which the initial fiber/matrix system present at the consolidation temperature T_0 is disassembled. The location of each constituent, at the reference temperature, is denoted by the solid lines. Upon cooling, both the fiber and matrix will contract (assuming their CTE's to be positive), with the matrix's contraction being greater than that of the fiber by an amount δ.

Superposition of fiber and matrix (by enforcing compatibility and thus eliminating this δ overlap) results in the development of stresses within the system. These stresses are such that the radial and circumferential fiber stresses are compressive, and the radial and circumferential matrix stresses are compressive and tensile, respectively. Consequently, the potential for the formation of radial cracks (fig. 2) exists due to the tensile hoop stress within the matrix. Whether or not cracking will occur clearly depends upon the magnitude of δ (CTE mismatch) and the ductility and strength of the matrix, or more

precisely, the fiber/matrix interface, because the maximum circumferential stress occurs at the interface and diminishes with the square of the radius (cf. equation A3 in appendix A).

Ideally, this problem could be avoided by the insertion of a layer of air δ thick between the fiber and matrix, thereby compensating for the mismatch in thermal strains attained during cooldown (see fig. 10(b)). In other words, the development of thermal stresses within the system can be mitigated by allowing unrestrained thermal strains to occur. Obviously, the value and manufacturing ability of such a composite system is unrealistic. However, this ideal situation does suggest that insertion of a material with the "proper character" between the fiber and matrix should minimize, if not eliminate, the buildup of thermal stresses within the plane (see fig. 10(c)).

As previously stated, the question at hand is the determination of this "proper character." Initially, if we restrict our attention to thermoelastic behavior, this character can be described mechanically by three parameters: the coefficient of thermal expansion, the thickness of the layer, and the stiffness. Utilization of figure 10 can provide insight with regard to the preferred magnitude of the unknown compliant layer's coefficient of thermal expansion (α^c), assuming a given thickness δ plus and stiffness E^c.

For example, if α^c is equal to α^f (the CTE of the fiber), a similar if not identical resistance to the contractive thermal strains within the matrix exists as in the system with no compliant layer. Alternatively, if the unknown layer were to possess an α^c such that it was between that of the fiber and matrix, some reduction in thermal strain mismatch (displacement δ) could be achieved. However, if the CTE of the unknown layer were greater than that of the matrix, the contraction of this layer would be greater than that of the matrix and thereby allow the matrix to contract freely. Restated, the unknown material would in essence "get out of the way" of the surrounding matrix material and thus resemble the ideal case in which no thermal stress is generated. Clearly , due to compatibility constraints, if α^c is sufficiently large and perfect bonding exists between the compliant layer and matrix, the matrix may indeed be pulled, or forced, to contract beyond the usual $\alpha^m \Delta T$ amount, thus inducing a tensile radial and compressive hoop stress state within the matrix. Such an argument would suggest that there exists an α^c (greater than α^m) and thickness combination which would eliminate the in–plane stress state within the matrix while increasing the stress in the fiber. Intuition also tells us that the stress state within the compliant layer will increase as α^c increases, given a fixed thickness and E^c, since in essence the load on the compliant layer is being increased.

Parametric Study

A parametric study was conducted involving the variation of the CTE, thickness, and modulus to substantiate the above observations relative to thermoelastic behavior. Selected results are presented in figures 11 to 14. Figures 11 and 12 illustrate the variation of circumferential and longitudinal residual stress (i.e., the stress attained upon reaching room temperature) as a function of the ratio of the CTE of the compliant layer and matrix (i.e., α^c/α^m), respectively. This CTE ratio can be extended to incorporate other fiber–reinforced systems by utilizing an alternative normalized CTE ratio; that is, $(\alpha^c-\alpha^f)/(\alpha^m-\alpha^f)$, wherein the driving α–mismatch between that of the fiber and matrix is incorporated.

The validity of the stresses shown correspond to the inner radius $r \cong a$ and $r \cong b$ for the matrix, respectively, while those associated with the fiber are valid for all locations within the fiber. Also included in the figures are the results for two normalized compliant layer thicknesses, t/a = 0.1 and 0.05, where t is the thickness of the compliant layer and a is the radius of the fiber. Note that the stresses reported in figures 11 and 12 are associated with a compliant layer whose modulus ($E^c=0.5E^m$) and Poisson ratio ($\nu^c=\nu^m$) are held fixed.

A comparison of these stress curves within any given material is not strictly valid since the location of the corresponding integration points, the inner radius, changes with a variation in compliant layer thickness. This variation is quite small, however, and for the purposes of this study such a comparison is justifiable.

An examination of figure 11 shows that increasing the normalized CTE ratio for a given thickness, t/a, decreases the circumferential stress in the matrix while increasing it in the compliant layer and fiber[3]. Furthermore, figure 11 illustrates that, for a given CTE ratio (e.g., $\alpha^c/\alpha^m = 2.0$), increasing the thickness, t/a, of the compliant layer results in a decrease in the magnitude of the circumferential stress within the matrix, compliant layer, and fiber. Similar (but less significant) trends with regard to the change in longitudinal stress are observed in figure 12. Figures 11 and 12 both illustrate a rapid increase in stress within the compliant layer as its CTE, α^c, is increased. Experience suggests that this increase could be compensated for by modifying the elastic stiffness, E^c, of the compliant layer.

---

[3]Note that a CTE ratio of 1.0 corresponds to the case when the CTE of the compliant layer and that of the matrix is the same, while a ratio equal to 0.392 corresponds to the case when the compliant layer's CTE is equal to that of the fiber.

Figures 13 and 14 illustrate the effect of varying the stiffness on the circumferential stress (σ_θ) distribution when a constant thickness, t/a=0.1, is specified. The effect on the radial distribution of σ_θ is summarized by plotting the hoop stress induced at both the inner radius, IR, and outer radius, OR, of the compliant layer cylinder (fig. 14). Two dominant trends are exhibited in figures 13 and 14. The first is that the magnitude of the circumferential stress for a given CTE ratio is significantly decreased within the compliant layer as well as within the fiber when the stiffness of the compliant layer is decreased, while the matrix remains basically unaffected for $\alpha^c/\alpha^m < 4$. The second trend deals with the increasing influence that stiffness, E^c, has on the resulting stress distribution (i.e., the difference between IR and OR stress magnitudes increases as stiffness increases) when the CTE of the compliant layer is increased.

Experimental data indicate that the matrix's yield stress is approximately 50 ksi at room temperature. It is therefore clear from the high stress values computed (those values greater than 50 ksi) in the compliant layer and matrix material that a purely thermoelastic analysis is insufficient to provide realistic results. Therefore, the next logical step is to incorporate yielding, or plasticity, of both the unknown compliant layer and the matrix material into the parametric stress analysis.

Summary of Thermoelastic Trends

A simple thought experiment was described to help explain and motivate the use of a larger CTE in the compliant layer than that in the matrix. Calculations showed that:

(1) Increasing the normalized CTE ratio of the compliant layer decreases the circumferential and longitudinal stress in the matrix while increasing it in the compliant layer and fiber.

(2) Increasing the thickness (t/a) of the compliant layer results in a decrease in the magnitude of circumferential and longitudinal stress within the matrix, compliant layer, and fiber. The longitudinal fiber stress is, however, increased beyond an α^c/α^m ratio of two.

(3) Decreasing the stiffness of the compliant layer has a significant impact on reducing the circumferential stress in the compliant layer and fiber, while the matrix stress is relatively unaffected.

(4) The influence of the stiffness increases as the CTE of the compliant layer is increased.

The reader is cautioned not to draw any definitive conclusions at this point since some important departures from the above trends are observed when plasticity is incorporated in the analysis, as illustrated in the next section.

THERMOELASTIC PLASTIC STRESS ANALYSIS

The incorporation of yielding, or plasticity, is accomplished by assuming a uniaxial bilinear stress–strain response of the matrix, as shown in figure 15 and table V. Note that the yield point denoted by σ_y^m is defined by using a 0.02% offset criterion, and H^m defines the linear hardening slope. The temperature–dependent material response determined experimentally by Brindley (refs. 11 and 13) for the Ti_3Al+Nb matrix clearly supports this assumption. Again the unknown compliant layer material properties are taken relative to that of the known matrix material throughout the temperature range E^c/E^m, σ_y^c/σ_y^m, and H^c/H^m. The multiaxial yield criterion utilized was that of von Mises. All stress analyses were performed numerically with the nonlinear finite element program MARC[4]

The inclusion of plasticity effects within the compliant layer and matrix were found to have a significant impact on the magnitude and distribution of stress within the composite system. This impact is best illustrated by example. For comparison purposes both the elastic and elastic–plastic calculations are shown in table VII, in which the distribution of radial, circumferential, and longitudinal stress versus radial location are tabulated, for the compliant layer idealization depicted in figure 5 with $\alpha^c/\alpha^m = 2.0$, $E^c/E^m=0.5$, $\sigma_y^c/\sigma_y^m=0.5$, and $H^c/H^m=0.5$. An examination of table VII reveals that inclusion of plasticity in the calculations results in approximately a 20 to 70 percent reduction in stress magnitudes when compared with the purely elastic calculations. As one might expect, the largest reductions are confined to areas of highest stress, or largest plastic strains, as in the compliant layer. Another point of interest is the redistribution of the longitudinal stress σ_z. In the elastic case, this stress is constant throughout a given material, while in the plastic case the stress drops at the inner radius due to the drop in radial and circumferential stress (see equation (1)) and then increases as one moves toward the outer radius. Note that in the matrix cylinder, σ_z approaches that value associated with a purely elastic solution. This is due to the fact that the outer radial region remains elastic until the final increment in temperature drop. Thus if ΔT were larger or the matrix softer, then σ_z at r=c would be lower, as illustrated later.

---

[4]A simplified analytical solution can be obtained if one assumes a Tresca yield criterion and assumes that $\sigma_r < \sigma_z < \sigma_\theta$. However, except for a small region near the inner radius of the compliant layer (table VII), this latter assumption is invalid for the majority of cases under investigation. Therefore, using the Tresca criterion does not provide the analyst with any greater analytical simplicity than use of the von Mises criterion.

Compliant Layer Thermoelastic Plastic Parametric Study

In light of including material nonlinearity, let us again examine the role of a compliant layer in reducing the overall residual stress field within a composite system, in particular, the tensile hoop stress which is believed to be linked to the radial cracking of the fiber–matrix interface. The problem definition discussed earlier and shown in figure 10 still applies and suggests that the CTE and thickness of the compliant layer will play the dominant role with regard to reducing the tensile hoop stress within the matrix.

This was investigated by varying the CTE, α^c, and thickness, t/a, of the compliant layer while holding the remaining available parameters E^c, σ_y^c, and H^c fixed. These parameters were taken to be 0.5 relative to those of the matrix throughout the temperature range E^c/E^m=0.5, $\sigma_y^c/\sigma_y^m = 0.5$, and $H^c/H^m = 0.5$.

Figures 16, 17, and 18 illustrate the variation of circumferential, longitudinal, and radial stress components for each constituent as a function of the normalized CTE ratio α^c/α^m, respectively. The stress values shown correspond to the inner radius for the compliant and matrix cylinder, while those associated with the fiber are valid for all radial locations within the fiber. Furthermore, results associated with four normalized compliant layer thicknesses (t/a = 0.05, 0.075, 0.1, and 0.2) are included in figures 16 to 18.

One can see from figure 16 that, for a given normalized thickness t/a, increasing the normalized CTE decreases the circumferential stress in the matrix and fiber while increasing the stress in the compliant layer. Notice that beyond a given CTE ratio (e.g., $\alpha^c/\alpha^m = 2.0$ for t/a = 0.1) the compliant layer hoop stress becomes greater than that of the matrix. The actual magnitude of this compliant layer stress component is immaterial at this stage, since with proper material selection this increase in stress can be controlled. This will become clear in the following section. The second major trend observed is that given a CTE ratio greater than 0.392, increasing the normalized thickness decreases the matrix and fiber hoop stress while increasing the compliant layer stress. As alluded to earlier, there appears to exist an α^c and thickness combination that can eliminate the tensile hoop stress in the matrix. Therefore, the net result of including a compliant layer is to lower, if not eliminate or change, the sign of the tensile hoop stress component of the matrix and fiber. Clearly this reduction is at the cost of increasing the compliant layer stress.

A comparison of figure 16 with its purely elastic counterpart (fig. 11) shows a number of differences. The first is the nonlinearity of the stress versus CTE curves corresponding to the elastic/plastic case when compared with those of the elastic. The second is that the fiber stress in the elastic cases increases with respect to increasing CTE, while the fiber stress corresponding to the plastic cases decreases. This reversal in trends can be explained by considering a fiber subjected to a pressure loading equal to $P^c = E^c \alpha^c \Delta T$. Thus, if α^c is increased while holding the stiffness and change in temperature constant, one would expect the stress in the fiber to increase as in figure 11. However, when plasticity is included, this pressure P^c is limited by the yielding of the material and in fact, due to the coupled kinematic effects, this pressure is actually reduced along with the stress within the fiber. The third difference is a subtle shift in the thickness dependence in the compliant layer stress. The fourth difference, as noted earlier, is an overall lowering of the stress values with the inclusion of plasticity. The general trend, however, remains intact with regard to reducing the matrix stress by increasing either the CTE or thickness of the compliant layer.

In examining the longitudinal stress versus normalized CTE ratio (fig. 17), one observes within all three constituent materials an increase in longitudinal stress with an increase in CTE ratio. The longitudinal stress in the matrix and fiber does, however, reverse this trend beyond a certain critical CTE ratio, determined by the change in sign of the sum of the circumferential and radial stress. Similarly, an increase in longitudinal stress is observed with an increase in normalized thickness (for a specified CTE ratio) in the matrix and compliant constituent materials. Note that increasing the thickness lowers the critical CTE at which the longitudinal stress in the matrix peaks out.

In comparing the trends indicated in figures 12 and 17, a number of differences are observed that are similar to those noted earlier for the circumferential stress. These include the nonlinear appearance of the curves in the plasticity case, the reversal in fiber stress with respect to increasing the CTE, a reversal in thickness dependence, and an overall reduction in stress levels with the inclusion of plasticity. The most important discrepancy between an elastic (fig. 12) and plastic (fig. 17) analysis resides in the trends in the matrix. In the elastic case, increasing the CTE ratio or normalized thickness decreases the longitudinal stress, whereas when plasticity is included, the stress is increased. This increases the potential for initiating cracking in the longitudinal direction. Provided loading is in the fiber direction, longitudinal cracking is considered to be more detrimental then radial cracking, thereby requiring that upper limits on both thickness and CTE of the compliant layer be imposed. These limits will be discussed later.

Figure 18 illustrates the effect on the radial stress distribution of varying the CTE and thickness of the compliant layer. Clearly, as the CTE and/or thickness are increased, the radial stress throughout the system is reduced. A comparison of trends resulting from an elastic (fig. 11) analysis with those from the plastic analysis reveals a nonlinear appearance in the curves for the plasticity case and a reduction, instead of an increase, in radial stress with respect to increasing CTE. This reduction in radial stress with increasing CTE suggests another potential problem regarding the use of compliant layers; that is, bond strength.

Throughout this study an assumption of perfect bonding has been made. However, in actuality, a wide range of bonding strengths can exist. For instance, if the bonding strength is purely mechanical (e.g., frictional), reducing the radial stress is proportional to reducing the bond strength, and therefore the load carrying capability, of the composite system. As a result, an upper limit on the allowable CTE and/or thickness of the compliant layer may be necessary if the bond strength at either interface is questionable. For example, if the bond strength is only frictional, then this limit would be reached when σ_r, the radial stress, becomes zero or tensile.

Effect of Varying Compliant Layer Material Parameters

In the previous section only variations in compliant layer CTE and thickness have been addressed, with all other parameters held fixed. As observed previously, increasing the CTE or thickness resulted in an increase in compliant layer stress in the longitudinal and circumferential directions. Therefore, the question at hand is what impact do the material properties of the compliant layer have on the resulting residual stress distribution. To answer this question, seventeen different sets of material parameters were investigated. Cases in which the stiffness, yield point, and hardening slope are all normalized with respect to the corresponding matrix properties are described in table VIII. Results indicating the radial, circumferential, and longitudinal stress at specific radial locations are shown for all seventeen cases in tables IX to XI. These results are associated with a specific normalized thickness, t/a = 0.1, and CTE ratio, $\alpha^c/\alpha^m = 2.0$.

It is apparent from these tables that variations in mechanical properties have little if any impact on the fiber (roughly 20 percent) and matrix (under 5 percent) stress state, while the compliant layer stress state is greatly (as much as 90 percent) affected. Therefore only the compliant layer stress state as a function of material property will be studied. The variation in circumferential and longitudinal compliant layer stress versus normalized hardening slope, yield point, and stiffness is illustrated in figures 19 to 21.

In figure 19, the effect of varying the hardening slope H^c/H^m (between 0 and 1) on the circumferential and longitudinal stress is shown, given a relative yield point σ_y^c/σ_y^m = 0.5 and stiffness E^c/E^m = 0.666. As expected, the perfectly plastic case (i.e., H^c/H^m = 0) gives the lowest stress state, while an increase in the hardening slope increases the stress state. Note also that increasing the hardening slope causes an increasing stress distribution; that is, the difference between the stress at the inner and outer radius increases.

Figure 20 illustrates the effect of varying the yield point σ_y^c/σ_y^m on the circumferential and longitudinal stress distribution for a given stiffness E^c/E^m = 0.666 and hardening slope H^c/H^m = 0.5. Again as one might suspect, the stress state is reduced as the yield point is reduced. The deviation between inner and outer radial stress values decreases with increasing yield for the circumferential component, while it increases with increasing yield for the longitudinal component.

Figure 21 illustrates the effect of varying the stiffness E^c/E^m on the compliant layer stress state, given a relative yield and hardening slope of 0.5. Once again it is observed that increasing the stiffness ratio increases (at a decreasing rate) the circumferential and longitudinal stress components. Note that only the value of stress, not the distribution, is affected by modification of the stiffness ratio, and that the percent increase or decrease is much less per increment in stiffness ratio than that of the yield or hardening slope.

To gain insight into the relative importance of each available material parameter with regard to reducing the stress state within the compliant layer, the circumferential and longitudinal stress components are put in ascending order, from minimum to maximum (table XII). Note that the material parameters corresponding to case number 16 produce the minimum stress state, both circumferentially and longitudinally, with respect to inner and outer radial location, while case number 2 produces the maximum stress values. Table XII also contains the ratio of material properties associated with each case number, similar to table VIII but listed in ascending order of the resulting stress values. Column 1 represents a measure of the interaction between the hardening slope and yield point of the material, and is associated with the sum of the two ratios. Clearly, the smaller this sum the lower the stress state within the compliant layer. Columns 2, 3, and 4 are associated with the relative yield point, hardening slope, and stiffness ratios, respectively, and, as in column 1, the lower the ratio (provided the other two ratios remain fixed) the lower the stress state within the compliant layer.

With regard to impact on the resulting residual stress state, the level of importance increases as one moves from the right column to the left. This level of importance is illustrated by considering cases in which columns 1 and 4 are the same while the yield and hardening ratios of columns 2 and 3 vary. Under these constraints, cases exist which indicate as one might expect that more importance should be placed upon having a lower yield point than upon having a lower hardening slope (see cases 1, 10, 14, and 15 in table XII). The inherent coupling between yield point and hardening slope is illustrated by cases 16, 4, and 11. This prompted the inclusion of a still more important parameter, namely, the sum of the yield point and hardening slope.

When examining cases 10 and 12, one might observe that an exception to the above level of importance is indicated in table XII. Here it is not the lower yield point that dictates the lower stress state but rather the hardening slope. As noted in table XII, however, this is true only for the circumferential and longitudinal stress components associated with the inner radius; those associated with the outer radius follow the above guidelines.

Summary of Trends

In review, calculations have shown that the CTE and thickness dominate when attempting to reduce in–plane fiber and matrix stress. More specifically, increasing the CTE and thickness of the compliant layer decreases the in–plane stress (σ_r,σ_θ) within the fiber and matrix while increasing the out–of–plane (σ_z) stress component. The compliant layer's stiffness E^c, yield point σ_y^c, and hardening slope H^c dominate when attempting to reduce the stress state within the compliant layer, and yet have little if any effect on the fiber or matrix stress state. Furthermore, it has been observed that, when selecting a compliant layer material, the properties should be chosen such that

(1) $\alpha^c > \alpha^m$

(2) t/a should be as large as other considerations allow

(3) $H^c/H^m + \sigma_y^c/\sigma_y^m$ should be small

(4) Yield point σ_y^c relative to matrix should be low

(5) Hardening slope H^c relative to matrix should be low

(6) Elastic stiffness E^c relative to matrix should be low

The above list is in order of importance, with respect to impact, for obtaining a minimum overall residual stress state. Differences between performing elastic and elastic–plastic

analyses have also been noted. These include

(1) Nonlinear appearance of the curves in the case of plasticity,

(2) Reversal in fiber stress and longitudinal matrix stress with respect to increasing the CTE, and

(3) Reversal in thickness dependence and an overall reduction in stress levels with the inclusion of plasticity.

MATERIAL SELECTION

Given the above material parameter guidelines, candidate compliant layer and/or diffusion barrier materials can be put forth. Prior to selecting these candidate materials, more quantitative bounds on the key parameters $\alpha^c/\alpha^m > 1.2$ and $0.1 < t/a < 0.2$ were obtained by calibrating the analysis with a compliant layer to one without a compliant layer (i.e., SiC/Ti_3Al+Nb).

Results of the fiber/matrix analysis indicated that the circumferential stress at the fiber/matrix interface was 44.5 ksi, while the longitudinal stress at the inner and outer radius of the matrix cylinder was 39 and 62 ksi, respectively. Experimental results indicate that radial cracks formed at the fiber–matrix interface in the SiC/Ti_3Al + Nb system, while few if any longitudinal cracks appeared. As a result, the present analysis is calibrated to the experimental observations by assuming that the fracture strength at the inner diameter of the matrix is equal to 44.5 ksi, while that at the outer diameter is greater than 62 ksi. In other words, a gradient in fracture strength is applied to the simplified analysis to account for the unknown interface properties as well as possible material defects in the actual system. Thus a circumferential stress greater than or equal to 44.5 would result in radial cracking, while a longitudinal stress less than 62 ksi would not result in axial cracking. The lower limit on the CTE ratio was determined by imposing this limit of $\sigma_\theta \leq 44.5$ on the curves of figure 16. Similarly, imposing the limit that $\sigma_z \leq 62$ on the curves of figure 17 gives the upper limit on the thickness. Note that the stress values given in figure 17 correspond to only those associated with the inner radial locations, although as shown in figure 22 the stress associated with the outer radial location corresponds to those of the inner just prior to the peaking of the longitudinal stress.

These bounds should not be considered absolutes, since the interface material in the actual SiC/Ti_3Al+Nb composite is unknown (thus critically affecting the stress values) and the given stress values are at room temperature (cracking could have initiated at a higher temperature and therefore lower stress). Furthermore, a lower upper bound on the

compliant layer thickness can be achieved based on overall composite density considerations.

Considering the above limits and the fact that processing temperatures are typically above 1500^{o}F (thus requiring a melting point in excess of 1500^{o}F), pure element and alloy candidate compliant/compensating layer materials are put forth in tables XIII and XIV, respectively. These candidates are limited still further by practical considerations such as handleability in air, radioactive elements, carcinogenic properties, and potentially too high a yield to maintain adequate stress levels in the compliant layer itself. Stars in the above tables indicate the affected candidate materials. With respect to pure elements, the candidates of choice appear to be silver, copper, and gold, with copper being the best of the three, in the authors' opinion, from a mechanics and economics standpoint.

Chemical compatibility with the fiber and matrix is probably the most restrictive criterion for a candidate compliant layer material. Thermodynamic studies (ref. 14) conducted on various candidate materials have revealed that copper is indeed the system of choice provided a diffusion barrier between the copper and Ti_3Al+Nb matrix is used. The diffusion barrier selected for the present study is niobium. This system will be fabricated by Textron and tested by Lewis personnel in order to experimentally verify the feasibility of the compliant layer concept.

DISCUSSION OF ISSUES AND FUTURE WORK

This report has taken us one step closer to understanding the advantages and disadvantages of employing a compliant/compensating layer. A number of issues still remain to be addressed. First is the effect of fiber interaction, spacing, and volume fraction. Second is the effect of warping (i.e., the removal of the assumption that planes remain plane) and fiber breakage. These must be examined since such a study would introduce longitudinal shears into the stress analysis and allow us to address the issue of circumferential debonding and load transfer (increase in critical length) caused by the inclusion of a compliant layer. Third is the effect of multiple compliant layers, since all conclusions stated in this report are valid only for a single layer. Fourth, the stress analysis must account for material time dependency during the fabrication cycle in order to accurately determine the true residual stress field and draw conclusions about optimum cooldown histories. This would require the inclusion of viscoplasticity in the stress analysis. Fifth, we must address the question of the fabricability and effectiveness of utilizing a thermally anisotropic interface layer whereby the radial and longitudinal CTE are different. The assumption here is that if the longitudinal CTE of the layer were

between that of the fiber and matrix, and the radial CTE were greater than the matrix, then the hoop stress within the matrix could be reduced while not adversely affecting the longitudinal stress. Lastly, prior to passing final judgment on the adequacy or inadequacy of utilizing a compliant layer, thermal cycling with and without a mechanical load needs to be addressed. This will be attempted by using the concept of shakedown. All of these areas are presently being investigated.

SUMMARY AND CONCLUSIONS

The present study has investigated both analytically and numerically the use of a compliant layer (or better named, compensating layer) concept to reduce, if not eliminate, residual stress buildup, and therefore cracking, during fabrication cooling. Significant effort has been devoted to understanding and describing the mechanics of the problem, specifically, the importance of the initial stress analysis assumptions. A detailed parametric study was performed using a finite element concentric cylinder model with generalized plane strain end conditions and free boundary conditions. The fiber, SiC, was assumed to be isotropic and linear elastic, while the unknown compliant layer and matrix (Ti_3Al+Nb) cylinders were assumed to be isotropic and bilinear elastic–plastic. The unknown compliant layer properties were taken to be relative to the corresponding known matrix properties over the full temperature range. Finally, perfect bonding between cylinders was also assumed and only the initial cooldown cycle was analyzed. Within the confines of these assumptions, the following general conclusions have been reached:

1. Plasticity was shown to have significant influence on the actual magnitude and distribution of stress (i.e., the resulting trends) and therefore must be included in the analysis.
2. A compliant/compensating layer can be used to reduce, if not eliminate, in–plane (σ_r,σ_θ) residual stresses within the fiber and matrix and therefore radial cracking as well.
3. With this decrease in in–plane stresses comes an increase in longitudinal stress, thus potentially initiating longitudinal cracking.
4. Similarly, if bonding was strictly mechanical, especially frictional, the reduction in radial stress with the addition of a compliant layer could be extremely detrimental to the overall composite performance.

5. The two most important interface layer parameters for reducing the matrix in–plane stresses are the CTE and thickness of the layer; thus the reason for the more appropriate name – compensating layer. These two parameters should be chosen such that $\alpha^c > \alpha^m$ and the thickness, t/a, is as large as other considerations will allow.

6. The mechanical properties (yield point, hardening slope, and stiffness) play the dominant role in reducing the stress state within the interface layer and should be chosen such that relative to the matrix they are as low as possible.

7. When selecting an interface material, the order of importance, with respect to impact, for obtaining a minimum overall residual stress state, is, $\alpha^c > \alpha^m$, t/a, $H^c/H^m + \sigma_y^c/\sigma_y^m$, σ_y^c, H^c, and E^c. Be aware, however, that this requirement may not provide maximum life under cyclic conditions.

8. A candidate system (SiC/Cu/Nb/Ti3Al+Nb) has been selected to be manufactured and tested experimentally to verify the applicability of employing a compliant/compensating layer technology.

ACKNOWLEDGMENTS

The authors wish to acknowledge Don Petrasek, Dave McDanels and Drs. Rebecca Mackay and Ajay Misra for their input regarding the material science related aspects of this report.

REFERENCES

1. Brindley P.K., Bartolotta P.A., and MacKay, R.A., " Thermal and Mechanical Fatigue of SiC/Ti_3Al + Nb", HITEMP Review 1989, NASA CP10039, 1989, pp. 52–1 to 52–14.

2. Vedula, M., Pangborn, R.N., and Queeney, R.A., " Modification of Residual Thermal Stress in a Metal–Matrix Composite with the Use of Tailored Interfacial Region", Composites, March 1988, pp. 133–137.

3. Chou, T.W., Kelly, A., and Okura, A., "Fiber–reinforced Metal Matrix Composites", Composites, July 1985, pp. 187–206.

4. Harris, B., "Shrinkage Stresses in Glass/Resin Composites", Journal of Materials Science, 13, 1987, pp. 173–177.

5. Ghosn, L.J. and Lerch, B.A., "Optimum Interface Properties for Metal Matrix Composites", NASA TM 102295, Aug. 1989.

6. Caruso, J.J., Chamis, C.C., and Brown, H.C., "Parametric Studies to Determine the Effect of Compliant Layers on Metal Matrix Composite Systems", NASA TM 102465, April 1990.

7. Russell, T., Engineering Materials Technology Laboratory, General Electric, Lynn, Mass., 1990.

8. Agarwal, B.D. and Broutman, L.J., "Analysis and Performance of Fiber Composites," John Wiley & Sons, 1980.

9. PATRAN II User Manual, PDA Engineering, Santa Ana, CA, 1984.

10. MARC, Revision K.3, MARC Analysis Research Corporation, Palo Alto, CA, 1988.

11. Brindley, P.K., Materials Division, NASA Lewis Research Center, Cleveland OH.

12. Giannetti, B., Textron Inc, Lowell, Mass.

13. Brindley, P.K., Draper, S.L., Nathal, M.V., and Eldridge, J.T., "Factors Which Influence Tensile Strength of a SiC/Ti–24Al–11Nb Composite," Proceedings of 1989 TMS Fall Meeting, Indianapolis, IN, Oct 1989.

14. Misra, A. , Materials Division, NASA Lewis Research Center, Cleveland, OH.

15. MathCAD, version 2.5, Mathsoft Inc., Cambridge, MA, 1989.

16. Naghdi, P.M., "Stress–Strain Relations in Plasticity and Thermo–plasticity," Plasticity, Proceedings of the Second Symposium on Naval Structural Mechanics, ed. E.H. Lee, P.S. Symonds, Pergamon Press, 1960.

APPENDIX A

By substituting equations (1), (2) and (4) to (6), one can obtain the general equations describing the radial displacement, u, and principal stress components, σ_r, σ_θ, σ_z, for a circular cylinder with generalized plane strain end conditions. These expressions are

$$u(r) = \frac{(1+\nu)}{(1-\nu)} \frac{\alpha}{r} \int_{r_i}^{r} Trdr + C_1 r + \frac{C_2}{r} \tag{A1}$$

$$\sigma_r(r) = \frac{-E}{(1-\nu)} \frac{\alpha}{r^2} \int_{r_i}^{r} Trdr + \frac{E}{(1+\nu)} \left[\frac{(C_1 + \nu e_z)}{(1-2\nu)} - C_2 \left(\frac{1}{r^2} \right) \right] \tag{A2}$$

$$\sigma_\theta(r) = \frac{E}{(1-\nu)} \frac{\alpha}{r^2} \int_{r_i}^{r} Trdr - \frac{E\alpha T}{(1-\nu)} + \frac{E}{(1+\nu)} \left[\frac{(C_1 + \nu e_z)}{(1-2\nu)} + C_2 \left(\frac{1}{r^2} \right) \right] \tag{A3}$$

$$\sigma_z = -\frac{E\alpha T}{(1+\nu)} + \frac{E}{(1-2\nu)(1+\nu)} \left[2\nu C_1 + (1-\nu) e_z \right] \tag{A4}$$

With the above expressions valid for a single circular cylinder, a variety of different laminated concentric cylinder models can be formulated by merely applying the appropriate boundary conditions to determine the constants of integration (C_1 and C_2).

Consider, for example, the three concentric cylinder case shown in figure 3(a) in which the generalized plane strain end and free surface boundary conditions are assumed. In this case, six unknown constants of integration (C_1 and C_2 corresponding to each constituent, i.e., fiber, compliant, and matrix cylinder) and the axial strain e_z must be determined before the radial displacement and three principle stress distributions will be known throughout the unit cell. Thus the seven boundary and compatibility conditions listed in table I must be satisfied.

Applying conditions (a) through (g) of table I to equations (A1), (A2), and (A4) results in the following seven constraint equations:

$$C_2^f = 0 \tag{a}$$

$$(C_1^c - C_1^f)a^2 + C_2^c = \frac{(1+\nu_f)}{(1-\nu_f)} \alpha_f \int_0^a T\, r dr \tag{b}$$

$$\left[\frac{E_c}{(1-2\nu_c)(1+\nu_c)}C_1^c - \frac{E_f}{(1-2\nu_f)(1+\nu_f)}C_1^f\right]a^2 - \frac{E_c}{(1+\nu_c)}C_2^c$$

$$-\left[\frac{E_f}{(1-2\nu_f)(1+\nu_f)}\nu_f - \frac{E_c}{(1-2\nu_c)(1+\nu_c)}\nu_c\right]a^2 e_z$$

$$= \frac{-E_f}{(1-\nu_f)}\alpha_f \int_0^a T\, r dr \qquad (c)$$

$$(C_1^m - C_1^c)b^2 + C_2^m - C_2^c = \frac{(1+\nu_c)}{(1-\nu_c)}\alpha_c \int_a^b T\, r dr \qquad (d)$$

$$\left[\frac{E_m}{(1-2\nu_m)(1+\nu_m)}C_1^m - \frac{E_c}{(1-2\nu_c)(1+\nu_c)}C_1^c\right]b^2$$

$$-\left[\frac{E_m}{(1+\nu_m)}C_2^m - \frac{E_c}{(1+\nu_c)}C_2^c\right]$$

$$-\left[\frac{E_c}{(1-2\nu_c)(1+\nu_c)}\nu_c - \frac{E_m}{(1-2\nu_m)(1+\nu_m)}\nu_m\right]b^2 e_z$$

$$= \frac{-E_c}{(1-\nu_c)}\alpha_c \int_a^b T\, r dr \qquad (e)$$

$$\frac{E_m}{(1-2\nu_m)(1+\nu_m)}C_1^m c^2 - \frac{E_m}{(1+\nu_m)}C_2^m + \frac{E_m}{(1-2\nu_m)(1+\nu_m)}\nu_m c^2 e_z$$

$$= \frac{-E_m}{(1-\nu_m)}\alpha_m \int_b^c T\, r dr \qquad (f)$$

$$\frac{E_m}{(1-2\nu_m)}\frac{\nu_m}{(1+\nu_m)}C_1^m(c^2-b^2) + \frac{E_c}{(1-2\nu_c)}\frac{\nu_c}{(1+\nu_c)}C_1^c(b^2-a^2) + \frac{E_f}{(1-2\nu_f)}\frac{\nu_f}{(1+\nu_f)}C_1^f a^2$$

$$+\left[\frac{E_m}{(1-2\nu_m)}\frac{(1-\nu_m)}{(1+\nu_m)}\frac{(c^2-b^2)}{2} + \frac{E_c}{(1-2\nu_c)}\frac{(1-\nu_c)}{(1+\nu_c)}\frac{(b^2-a^2)}{2}\right.$$

$$+\left.\frac{E_f(1-\nu_f)}{(1-2\nu_f)(1+\nu_f)}\frac{a^2}{2}\right]e_z$$

$$=\left[\frac{E_f}{(1-\nu_f)}\alpha_f a^2+\frac{E_c}{(1-\nu_c)}\alpha_c(b^2-a^2)+\frac{E_m}{(1-\nu_m)}\alpha_m(c^2-b^2)\right]\frac{T}{2} \qquad (g)$$

Writing the nontrivial equations (equations (b) to (g)) in matrix form results in:

$$[M]\{X\} = \{R\}$$

which can be solved by a simple inversion process; that is,

$$\{X\} = [M]^{-1}\{R\}$$

where the vector $\{X\}^T = \{C_1^f, C_1^c, C_2^c, C_1^m, C_2^m, e_z\}$ contains the constants of integration for equations (A1) to (A4). The solution to this system, as well as the displacement and stress field within each cylinder, has been accomplished by using the software package MATHCAD (ref. 15). The MATHCAD document containing the above details is given below. Similar boundary conditions can be applied to obtain displacement and stress distributions for the other boundary conditions discussed in this report.

MATHCAD DOCUMENT

ANALYTICAL SOLUTION FOR CONCENTRIC CYLINDER MODEL - THREE MATERIALS
INNER:FIBER; MIDDLE:COMPLIANT; OUTER:MATRIX
---- Generalized plane strain assumption------
---- Free surface constraints -------

DEFINE MATERIAL PROPERTIES AT ROOM TEMPERATURE; REFERENCE TEMPERATURE IS AT 1500 F

FIBER	MATRIX	COMPLIANT LAYER
EF := 58000.	EM := 16000.	RE := 0.5
AF := $1.96 \cdot 10^{-6}$	AM := $5.0 \cdot 10^{-6}$	RA := 2.0
VF := .25	VM := .26	VC := 0.26
		EC := EM · RE
		AC := RA · AM

DEFINE GEOMETRY AND TEMPERATURE CHANGE

fiber OD	compliant OD	matrix OD
a := 0.632	b := 0.6952	c := 1.0

change in temp	absolute DT
DT := -1425.	ABDT := 1425

SOLUTION OF CONSTANTS OF INTEGRATION

Fiber

$$A := AF \cdot \frac{EF}{1 - VF}$$

$$B := \frac{EF}{(1 + VF) \cdot (1 - 2 \cdot VF)}$$

Matrix

$$C := AM \cdot \frac{EM}{1 - VM}$$

$$D := \frac{EM}{1 + VM}$$

$$DM := \frac{EM}{(1 + VM) \cdot (1 - 2 \cdot VM)}$$

Compliant layer

$$CC := AC \cdot \frac{EC}{1 - VC}$$

$$CD := \frac{EC}{1 + VC}$$

$$CDM := \frac{EC}{(1 + VC) \cdot (1 - 2 \cdot VC)}$$

Longitudinal strain (left side)

$$EZ6 := B \cdot (1 - VF) \cdot \frac{a^2}{2} + CDM \cdot (1 - VC) \cdot \frac{b^2 - a^2}{2} + DM \cdot (1 - VM) \cdot \frac{c^2 - b^2}{2}$$

Longitudinal strain (right side)

$$REZ := A \cdot a^2 + CC \cdot \left[b^2 - a^2\right] + C \cdot \left[c^2 - b^2\right]$$

APPLY BOUNDARY CONDITIONS TO FORM MATRIX AND OBTAIN APPROPRIATE COEFFICIENTS

$$M26 := \left[\frac{-B}{CD} \cdot VF + \frac{VC}{1 - 2 \cdot VC}\right]$$

$$M36 := \left[\frac{-CDM}{D} \cdot VC + \frac{VM}{1 - 2 \cdot VM}\right]$$

$$M := \begin{bmatrix} -a^2 & a^2 & 1 & 0 & 0 & 0 \\ \frac{-B}{CD} \cdot a^2 & \frac{a^2}{1 - 2 \cdot VC} & -1 & 0 & 0 & M26 \cdot a^2 \\ 0 & -b^2 & -1 & b^2 & 1 & 0 \\ 0 & \frac{-CDM}{D} \cdot b^2 & \frac{CD}{D} & \frac{b^2}{1 - 2 \cdot VM} & -1 & M36 \cdot b^2 \\ 0 & 0 & 0 & \frac{c^2}{1 - 2 \cdot VM} & -1 & \frac{VM}{1 - 2 \cdot VM} \cdot c^2 \\ B \cdot VF \cdot a^2 & CDM \cdot VC \cdot \left[b^2 - a^2 \right] & 0 & DM \cdot VM \cdot \left[c^2 - b^2 \right] & 0 & EZ6 \end{bmatrix}$$

define the right-hand side

$$DT2 := \frac{DT}{2.0}$$

$$R := \begin{bmatrix} \frac{1 + VF}{1 - VF} \cdot AF \cdot DT2 \cdot a^2 \\ \frac{-A}{CD} \cdot DT2 \cdot a^2 \\ \frac{1 + VC}{1 - VC} \cdot AC \cdot DT2 \cdot \left[b^2 - a^2 \right] \\ \frac{-CC}{D} \cdot DT2 \cdot \left[b^2 - a^2 \right] \\ \frac{1 + VM}{1 - VM} \cdot AM \cdot DT2 \cdot \left[c^2 - b^2 \right] \\ REZ \cdot DT2 \end{bmatrix}$$

System of equations written in matrix notation

$$X := M^{-1} \cdot R$$

X contains the constants of integration
X={C1f,C1c,C2c,C1m,C2m,ez}

set-up increments in radial location

$N := 10 \qquad i := 0 \,..N \qquad rc_0 := a \qquad rc_{10} := b \qquad rm_0 := b$

fiber

$$rf_i := \frac{a}{N} \cdot i$$

compliant layer

$$rc_i := \frac{b - a}{N} \cdot i + a$$

matrix

$$rm_i := \frac{c - b}{N} \cdot i + b$$

---------- FIBER ----------

radial displacment

$$Uf_i := \frac{1 + VF}{1 - VF} \cdot AF \cdot \frac{DT}{2.0} \cdot rf_i + X_0 \cdot rf_i \qquad \text{eqn (A-1)}$$

radial stress

$$SRf := -A \cdot \frac{DT}{2.0} + B \cdot X_0 + B \cdot VF \cdot X_5 \qquad \text{eqn (A-2)}$$

hoop stress

$$STf := \frac{-A}{2.0} \cdot DT + B \cdot X_0 + B \cdot VF \cdot X_5 \qquad \text{eqn (A-3)}$$

longitudinal stress

$$SZf := -A \cdot DT + B \cdot 2.0 \cdot VF \cdot X_0 + B \cdot (1 - VF) \cdot X_5 \qquad \text{eqn (A-4)}$$

--------- COMPLIANT LAYER ----------

radial displacment

$$Uc_i := \frac{1 + VC}{1 - VC} \cdot AC \cdot \frac{DT}{2.0} \cdot \left[rc_i - \frac{a^2}{rc_i} \right] + X_1 \cdot rc_i + \frac{X_2}{rc_i}$$

radial stress

$$SRc_i := -CC \cdot \frac{DT}{2.0} \cdot \left[1.0 - \left[\frac{a}{rc_i} \right]^2 \right] + CD \cdot \left[\frac{X_1}{1 - 2 \cdot VC} - \frac{X_2}{\left[rc_i \right]^2} \right] + CDM \cdot VC \cdot X_5$$

hoop stress

$$STc_i := CC \cdot \frac{DT}{2.0} \cdot \left[1.0 - \left[\frac{a}{rc_i} \right]^2 \right] + CD \cdot \left[\frac{X_1}{1 - 2 \cdot VC} + \frac{X_2}{\left[rc_i \right]^2} \right] - CC \cdot DT + CDM \cdot VC \cdot X_5$$

longitudinal stress

$$SZc := -CC \cdot DT + CD \cdot 2.0 \cdot \frac{VC}{(1 - 2 \cdot VC)} \cdot X_1 + CDM \cdot (1 - VC) \cdot X_5$$

--------- MATRIX ----------

radial displacement

$$Um_i := \frac{1 + VM}{1 - VM} \cdot AM \cdot \frac{DT}{2.0} \cdot \left[rm_i - \frac{b^2}{rm_i} \right] + X_3 \cdot rm_i + \frac{X_4}{rm_i}$$

radial stress

$$SRm_i := -C \cdot \frac{DT}{2.0} \cdot \left[1.0 - \left[\frac{b}{rm_i} \right]^2 \right] + D \cdot \left[\frac{X_3}{1 - 2 \cdot VM} - \frac{X_4}{\left[rm_i \right]^2} \right] + DM \cdot VM \cdot X_5$$

hoop stress

$$STm_i := C \cdot \frac{DT}{2.0} \cdot \left[1.0 - \left[\frac{b}{rm_i} \right]^2 \right] + D \cdot \left[\frac{X_3}{1 - 2 \cdot VM} + \frac{X_4}{\left[rm_i \right]^2} \right] - C \cdot DT + DM \cdot VM \cdot X_5$$

longitudinal stress

$$SZm := -C \cdot DT + D \cdot 2.0 \cdot \frac{VM}{(1 - 2 \cdot VM)} \cdot X_3 + DM \cdot (1 - VM) \cdot X_5$$

APPENDIX B

ELASTIC

Assuming temperature–dependent material properties (i.e., E(T) and $\alpha(T)$) the stress–strain relations in equation (1) become:

$$\Delta\sigma_r = \frac{E}{(1-2\nu)(1+\nu)}\{(1-\nu)\Delta e_r + \nu(\Delta e_\theta+\Delta e_z) - (1+\nu)\alpha\Delta T\}$$

$$+ \frac{\Delta E}{(1-2\nu)(1+\nu)}\{(1-\nu)e_r + \nu(e_\theta+e_z) - (1+\nu)\alpha(T-T_o)\}$$

$$- \frac{E}{(1-2\nu)}\Delta\alpha(T-T_o) \qquad (B1)$$

$$\Delta\sigma_\theta = \frac{E}{(1-2\nu)(1+\nu)}\{(1-\nu)\Delta e_\theta + \nu(\Delta e_r+\Delta e_z) - (1+\nu)\alpha\Delta T\}$$

$$+ \frac{\Delta E}{(1-2\nu)(1+\nu)}\{(1-\nu)e_\theta + \nu(e_r+e_z) - (1+\nu)\alpha(T-T_o)\}$$

$$- \frac{E}{(1-2\nu)}\Delta\alpha(T-T_o) \qquad (B2)$$

$$\Delta\sigma_z = \nu(\Delta\sigma_r+\Delta\sigma_\theta) + E(\Delta e_z - \alpha\Delta T) + \Delta E(e_z - \alpha(T-T_o))$$

$$-\Delta\alpha\, E(T-T_o) \qquad (B3)$$

where Δ indicates an incremental change in the variable for a given increment in temperature (ΔT). Upon examining the above equations, one can sense the importance of including the effect of temperature–dependent material properties when ΔE and $\Delta\alpha$ are large; that is, when E and α are strongly temperature–dependent.

ELASTIC – PLASTIC

Similarly, if we assume temperature–dependent elastic–plastic behavior, the multi–axial incremental stress–strain equations can be written in index notation (ref. 16) as follows:

$$\dot{\sigma}_{ij} = D_{ijkl}(T)\,\dot{\epsilon}^e_{kl} + C_{ij}\,\dot{T} \qquad (B4)$$

where

$$C_{ij} = \frac{\partial D_{ijkl}(T)}{\partial T}\,\epsilon^e_{kl}$$

Decomposing the increment of total strain into an additive sum of elastic, plastic, and thermal contributions

$$\dot{e}_{ij} = \dot{\epsilon}^{e}_{ij} + \dot{\epsilon}^{p}_{ij} + \dot{\epsilon}^{th}_{ij}$$

$$\dot{\epsilon}^{e}_{ij} = \dot{e}_{ij} - \dot{\epsilon}^{p}_{ij} - \dot{\epsilon}^{th}_{ij} \qquad \text{(B5)}$$

and assuming a Von Mises yield condition, the increment in plastic strain is defined as

$$\dot{\epsilon}^{p}_{ij} = d\lambda \, S_{ij}$$

where
$$d\lambda = \frac{S_{ij} D_{ijkl} (\dot{e}_{kl} - \dot{\epsilon}^{th}_{kl}) + (S_{ij} C_{ij} - \frac{2}{3} Y \frac{\partial Y}{\partial T}) \dot{T}}{\frac{4}{9} Y \frac{\partial Y}{\partial E^{p}} + S_{mn} D_{mnpq} S_{pq}}$$

and taking

$$\dot{\epsilon}^{th}_{ij} = \alpha_{ij} \dot{T} \qquad \text{(B6)}$$

with
$$\alpha_{ij} = \alpha^{AV}_{ij} + \frac{\partial \alpha_{ij}}{\partial T}(T - T_o)$$

Given the above, we obtain the following expression for the stress rate,

$$\dot{\sigma}_{ij} = L_{ijkl}(T) \dot{e}_{kl} + H_{ij} \dot{T}$$

where

$$L_{ijkl} = D_{ijkl} - \frac{D_{ijmn} S_{mn} S_{pq} D_{pqkl}}{b}$$

$$H_{ij} = C_{ij} - L_{ijkl} \alpha_{kl} - \frac{D_{ijkl} S_{kl} (S_{pq} C_{pq} - \frac{2}{3} Y \frac{\partial Y}{\partial T})}{b}$$

and

$$b = \frac{4}{9} Y \frac{\partial Y}{\partial E^{p}} + S_{mn} D_{mnpq} S_{pq}$$

where Y and E^p are the equivalent yield stress and plastic strain, respectively. Again it is

apparent that if D_{ijkl}, α_{ij}^{AV} and Y are strongly dependent upon temperature, their influence should be taken into account.

TABLE I. - BOUNDARY CONDITIONS FOR A CONCENTRIC CYLINDER MODEL WITH THREE CONSTITUENTS, FREE SURFACE CONSTRAINT, AND GENERALIZED PLANE STRAIN END CONSTRAINTS

Location, r	Condition
0	$u^f(0)$ = finite value
a	$u^f(a) = u^c(a)$
a	$\sigma_r^f(a) = \sigma_r^c(a)$
b	$u^c(b) = u^m(b)$
b	$\sigma_r^c(b) = \sigma_r^m(b)$
c	$\sigma_r^m(c) = 0$

and equilibrium in the z direction, i.e.,

$$\int_0^a \sigma_z^f \pi r \, dr + \int_a^b \sigma_z^c \pi r \, dr + \int_b^c \sigma_z^m \pi r \, dr = 0$$

where superscripts f, c, and m represent the displacement and stresses corresponding to the fiber, compliant layer, and matrix cylinders, respectively.

TABLE II. - COMPARISON OF SURFACE AND END BOUNDARY CONDITIONS SHOWN IN FIGURE 3, CONSIDERING TEMPERATURE-INDEPENDENT ANALYTICAL SOLUTION PROCEDURE

End conditions	Location, r	Surface constraint					
		Free boundary			Homogenized		
		Stress, ksi					
		σ_r	σ_θ	σ_z	σ_r	σ_θ	σ_z
Plane strain ($\varepsilon_z = 0$)	Fiber	-32.8	-32.8	145.6	-----	-----	------
	Matrix:				-----	-----	------
	r = a	-32.8	76.5	125.4	-----	-----	------
	r = b	-23.4	67.0	125.4	-----	-----	------
	r = c	0	45.1	125.4	-----	-----	------
	Fiber	-29.5	-29.5	147.2	-----	-----	------
	Compliant layer:						
	r = a	-29.5	111.0	135.2	-----	-----	------
	r = b	-17.3	98.8	135.2	-----	-----	------
	Matrix:						
	r = b	-17.3	49.7	122.4	-----	-----	------
	r = c	0	33.4	122.4	-----	-----	------
Generalized plane strain ($\varepsilon_z \neq 0$)	Fiber	-32.6	-32.6	-90.4	-37.5	-37.5	-125.4
	Matrix:						
	r = a	-32.6	76.0	60.1	-37.5	73.2	49.2
	r = b	-23.2	66.5	60.1	-27.9	63.7	49.2
	r = c	0	44.7	60.1	-4.3	40.0	49.2
	Fiber	-29.3	-29.3	-93.6	-34.9	-34.9	-129.6
	Compliant layer:						
	r = a	-29.3	110.7	101.9	-34.9	108.2	95.2
	r = b	-17.1	98.6	101.9	-22.6	95.9	95.2
	Matrix:						
	r = b	-17.1	49.2	55.8	-22.6	45.6	44.4
	r = c	0	33.1	55.8	-5.0	28.0	44.4

TABLE III. - GEOMETRY, LOAD, AND MATERIAL PARAMETERS FOR ANALYSES ASSOCIATED WITH TABLE II

[Radii: a = 0.632; b = 0.6952; c = 1.0. Compliant layer thickness, t/a = 0.1; temperature difference, ΔT = -1425 °F; matrix yield at room temperature, σ_y^m = 53.89 ksi.]

Material property	Fiber	Compliant layer	Matrix
Coefficient of thermal expansion, α, in./in./°F	1.96×10^{-6}	10.0×10^{-6}	5.0×10^{-6}
Modulus of elasticity, E, Msi	58	8.0	16
Poisson ratio, ν	0.25	0.26	0.26

TABLE IV. - COMPARISON BETWEEN ASSUMPTION OF COUPLING AND DECOUPLING LONGITUDINAL STRESS TO IN-PLANE STRESSES FOR THREE COMPLIANT LAYER THICKNESSES (i.e., t/a = 0, 0.12, AND 0.2.) subjected to ΔT = 1472 °F

Matrix (inner radius)	No compliant layer (t/a = 0): a = b = 1.0; c = 1.58			Compliant layer (t/a = 0.12): a = 1.0; b = 1.12; c = 1.77			Compliant layer (t/a = 0.2): a = 1.0; b = 1.2; c = 1.897		
	Decoupled	Coupled	Difference,[a] percent	Decoupled	Coupled	Difference,[a] percent	Decoupled	Coupled	Difference,[a] percent
σ_r	-28.7	-29.77	3.6	-22.77	-26.85	15	-20.0	-25.32	21
σ_θ	66.8	69.57	4	53.2	62.7	16	46.7	59.12	21
σ_z	46.9	59.53	21.2	41.62	55.58	25	38.1	53.2	28
e_z	-0.005167	-0.005204	0.7	-0.005423	-0.005457	0.6	-0.00563	-0.005617	0.2

[a]Difference is found by $(\sigma^{coupled} - \sigma^{decoupled})/\sigma^{coupled}$.

Material property	Fiber	Compliant layer	Matrix
Coefficient of thermal expansion, α, in./in./°F	2.72×10^{-6}	4.38×10^{-6}	6.5×10^{-6}
Modulus of elasticity, E, Msi	62	10	10.9
Poisson ratio, ν	0.25	0.30	0.30

TABLE V. - EXPERIMENTALLY OBTAINED (SEE REFS. 11 AND 12) TEMPERATURE-DEPENDENT FIBER AND MATRIX MATERIAL PROPERTIES

(a) Fiber (SiC; SCS-6)

Material property	Temperature, °F				
	77	214	398	571	753
Coefficient of thermal expansion, α, in./in./°F	1.96×10^{-6}	1.98×10^{-6}	2.01×10^{-6}	2.07×10^{-6}	2.15×10^{-6}
Modulus of elasticity, E, Msi	58	58	58	58	58
Poisson ratio, ν	0.25	0.25	0.25	0.25	0.25

Material property	Temperature, °F				
	932	1109	1296	1472	1652
Coefficient of thermal expansion, α, in./in./°F	2.24×10^{-6}	2.33×10^{-6}	2.42×10^{-6}	2.48×10^{-6}	2.55×10^{-6}
Modulus of elasticity, E, Msi	58	58	58	58	58
Poisson ratio, ν	0.25	0.25	0.25	0.25	0.25

(b) Matrix (Ti-24Al-11Nb)

Material property	Temperature, °F					
	75	392	797	1112	1202	1500
Coefficient of thermal expansion, α, in./in./°F	5.0×10^{-6}	5.2×10^{-6}	5.7×10^{-6}	5.85×10^{-6}	5.9×10^{-6}	6.15×10^{-6}
Modulus of elasticity, E, Msi	16.0	14.5	11.0	12.5	9.89	6.2
Stress, σ_y, ksi	53.89	59.0	53.7	42.2	39.1	24.0
Hardening slope, H, Msi	3.333	0.441	0.322	0.187	0.097	0
Poisson ratio, ν	0.26	0.26	0.26	0.26	0.26	0.26

TABLE VI. - COMPARISON BETWEEN STRESS RESULTS USING TEMPERATURE-DEPENDENT AND TEMPERATURE-INDEPENDENT MATERIAL PROPERTIES

[$t/a = 0.1$; $E^c/E^m = \sigma_y^c/\sigma_y^m = H^c/H^m = 0.5$.]

Location	Temperature-dependent properties			Temperature-independent properties			Difference,[a] percent		
	σ_r	σ_θ	σ_z	σ_r	σ_θ	σ_z	r	θ	z
Fiber	-33.0	-33.0	-105.0	-29.4	-29.4	-93.7	10.9	10.9	10.7
Compliant layer:									
Inner radius (r = 0.636)	-30.6	122.1	114.2	-27.3	109.1	102.0	10.8	10.6	↓
Outer radius (r = 0.683)	-20.4	112.0	114.2	-18.2	100.0	102.0	10.7	10.7	↓
Matrix:									
Inner radius (r = 0.721)	-16.0	52.2	114.2	-14.3	46.6	55.9	10.6	10.7	↓
Outer radius (r = 0.964)	-1.0	37.2	62.6	-.9	33.2	55.9	10	10.7	↓

[a]Difference found by $[()^{dependent} - ()^{independent})]/()^{dependent}$.

TABLE VII. - COMPARISON OF ELASTIC AND ELASTIC-PLASTIC STRESS ANALYSIS RESULTS

[$t/a = 0.1$; $E^c/E^m = \sigma_y^c/\sigma_y^m = H^c/H^m = 0.5$.]

Material	Location, r	Radial stress, σ_r			Circumferential stress, σ_θ			Longitudinal stress, σ_z		
		Elastic	Plastic	Difference,[a] percent	Elastic	Plastic	Difference,[a] percent	Elastic	Plastic	Difference,[a] percent
Fiber	0.14	-33.0	-19.0	42	-33.0	-19.0	42	-105	-83	21
	.24	↓	↓	↓	↓	↓	↓	↓	↓	↓
	.37	↓	↓	↓	↓	↓	↓	↓	↓	↓
	.53	↓	↓	↓	↓	↓	↓	↓	↓	↓
Compliant layer	0.64	-30.6	-18.4	41	122	36.8	70	114	34.9	69
	.65	-27.0	-16.8	38	118	36.2	82	↓	35.6	69
	.67	-23.6	-15.6	34	115	35.7	69	↓	36.4	68
	.68	-20.4	-14.4	29	112	35.3	68	↓	37.1	67
Matrix	0.72	-16.0	-11.7	27	52.2	35.2	33	62.6	51.9	17
	.78	-10.9	-8.1	26	47.1	33.5	29	↓	55.6	11
	.84	-6.9	-5.2	25	43.1	31.7	26	↓	58.4	7
	.90	-3.7	-2.6	30	39.8	30.0	25	↓	60.6	3
	.96	-1.0	-.5	50	37.2	28.5	23	↓	62.3	.5

[a]Difference is found by $(\sigma^{elastic} - \sigma^{plastic})/\sigma^{elastic}$.

TABLE VIII. - CASES ("UNKNOWN" COMPLIANT LAYER MATERIAL PROPERTIES) INVESTIGATED RELATIVE TO MATRIX MATERIAL PROPERTIES

Case	E^c/E^m	σ_y^c/σ_y^m	H^c/H^m
1	0.5	0.5	0.5
2	1.25	1.0	1.0
3	1.25	1.0	.25
4	.666	.5	.25
5	1.25	.75	1.0
6	1.0	.5	1.0
7	1.0	.5	.5
8	1.0	1.0	1.0
9	.666	.666	.5
10	↓	.75	.25
11	↓	.375	.5
12	↓	.5	↓
13	↓	.75	↓
14	↓	1.0	↓
15	↓	.5	1.0
16	↓	.5	0
17	1.25	.5	.5

TABLE IX. - RADIAL RESIDUAL STRESSES AT INDICATED RADIAL LOCATIONS FOR VARIOUS CASES DESCRIBED IN TABLE VIII

[t/a = 0.1 and α^c/α^m = 2.0.]

Case	Location				
	Fiber	Compliant layer		Matrix	
		Inner radius	Outer radius	Inner radius	Outer radius
	Radial stress, σ_r, ksi				
1	-19.0	-18.1	-14.4	-11.7	-0.5
2	-24.4	-22.7	-15.0	-11.9	-.6
3	-20.2	-19.1	-14.2	-11.4	-.5
4	-17.5	-16.8	-13.8	-11.3	-.5
5	-23.3	-21.6	-14.8	-11.7	-.6
6	-21.9	-20.5	-14.7	-11.7	-.55
7	-19.1	-18.2	-14.0	-11.4	-.5
8	-24.2	-22.5	-15.2	-12.0	-.6
9	-20.0	-18.9	-14.5	-11.7	-.5
10	-19.0	-18.1	-14.2	-11.5	↓
11	-18.4	-17.6	-14.1	-11.4	↓
12	-19.1	-18.2	-14.2	-11.5	↓
13	-20.4	-19.3	-14.6	-11.8	↓
14	-21.7	-20.5	-15.0	-12.0	-.6
15	-21.3	-20.1	-14.9	-11.9	-.5
16	-15.6	-15.2	-13.3	-10.9	-.5
17	-19.1	-18.1	-13.9	-11.3	-.5

TABLE X. - CIRCUMFERENTIAL RESIDUAL STRESSES AT INDICATED RADIAL LOCATIONS FOR VARIOUS CASES DESCRIBED IN TABLE VIII

[t/a = 0.1 and α^c/α^m = 2.0.]

Case	Location				
	Fiber	Compliant layer		Matrix	
		Inner radius	Outer radius	Inner radius	Outer radius
	Circumferential stress, σ_θ, ksi				
1	-19.0	36.8	35.3	35.2	28.5
2	-24.4	89.7	86.8	35.5	28.9
3	-20.2	52.1	52.5	34.4	27.7
4	-17.5	27.0	26.5	34.1	27.3
5	-23.3	79.7	76.4	35.2	28.6
6	-21.9	66.3	62.7	35.2	28.6
7	-19.1	42.4	40.8	34.4	27.6
8	-24.2	85.2	82.3	35.9	29.4
9	-20.0	46.1	44.8	35.2	28.5
10	-19.0	38.0	38.0	34.7	28.1
11	-18.4	34.5	32.7	34.6	27.8
12	-19.1	39.5	37.9	34.8	28.1
13	-20.4	49.5	48.3	35.3	28.8
14	-21.7	59.5	58.7	35.8	29.4
15	-21.3	57.3	54.9	35.8	29.2
16	-15.6	11.9	12.8	33.2	26.4
17	-19.1	43.7	42.1	34.1	27.3

TABLE XI. - LONGITUDINAL RESIDUAL STRESSES AT INDICATED RADIAL LOCATIONS FOR VARIOUS CASES DESCRIBED IN TABLE VIII

[t/a = 0.1 and α^c/α^m = 2.0.]

Case	Location				
	Fiber	Compliant layer		Matrix	
		Inner radius	Outer radius	Inner radius	Outer radius
	Longitudinal stress, σ_z, ksi				
1	-82.9	34.9	37.1	51.9	62.2
2	-92.9	84.9	89.7	51.2	61.8
3	-86.4	50.1	55.5	52.2	62.0
4	-81.3	25.8	28.3	52.6	62.2
5	-91.0	75.2	78.8	51.4	61.9
6	-88.3	62.2	64.5	51.6	62.0
7	-84.2	40.3	42.9	52.3	62.1
8	-92.0	80.8	85.3	51.0	61.9
9	-84.8	43.9	47.1	51.8	62.2
10	-83.4	36.5	40.3	52.2	↓
11	-82.5	32.6	34.3	52.3	
12	-83.5	37.4	39.8	52.1	
13	-85.4	47.2	50.7	51.7	
14	-87.3	56.9	61.6	51.3	62.1
15	-86.6	53.8	56.8	51.4	62.1
16	-78.7	11.5	14.3	53.1	62.2
17	-84.5	41.7	44.3	52.4	62.1

TABLE XII. - ORDERING OF CIRCUMFERENTIAL AND LONGITUDINAL COMPLIANT LAYER STRESS COMPONENTS FROM MINIMUM TO MAXIMUM VALUES

[$t/a = 0.1$ and $\alpha^c/\alpha^m = 2.0$.]

Case	Inner radius	Outer radius	Inner radius	Outer radius	Corresponding material properties			
	Circumferential stress, σ_θ, ksi		Longitudinal stress, σ_z, ksi		$H^c/H^m + \sigma_y^c/\sigma_y^m$ (1)	σ_y^c/σ_y^m (2)	H^c/H^m (3)	E^c/E^m (4)
16	11.9	12.8	11.5	14.3	0.5	0.5	0	0.666
4	27.0	26.5	25.8	28.3	.75	.5	.25	.666
11	34.5	32.7	32.6	34.3	.875	.375	.5	.666
1	36.8	35.3	34.9	37.1	1.0	.5	.5	.5
10	38.0	38.0[a]	36.5	40.3[a]	↓	.75	.25	.666
12	39.5	37.9[a]	37.4	39.8[a]		.5	.5	.666
7	42.4	40.8	40.3	42.9		.5	↓	1.0
17	43.7	42.1	41.7	44.3	↓	.5		1.25
9	46.1	44.8	43.9	47.1	1.16	.666		.666
13	49.5	48.3	47.2	50.7	1.25	.75	↓	.666
3	52.1	52.5	50.1	55.5	1.25	1.0	.25	1.25
15	57.3	54.9	53.8	56.8	1.5	.5	1.0	.666
14	59.5	58.7	56.9	61.6	1.5	1.0	.5	.666
6	66.3	62.7	62.2	64.5	1.5	.5	1.0	1.0
5	79.7	76.4	75.2	78.8	1.75	.75	↓	1.25
8	85.2	82.3	80.8	85.3	2.0	1.0		1.0
2	89.7	86.8	84.9	89.7	2.0	1.0	↓	1.25

[a]The only exceptions to the ordering.

TABLE XIII. - PURE-ELEMENT CANDIDATE COMPLIANT LAYER MATERIALS FOR SCS-6/Ti_3Al + Nb COMPOSITE SYSTEM

Element	Coefficient of thermal expansion, α/α^m	Yield stress, σ_y/σ_y^m	Modulus of elasticity, E/E^m	Melting point, °F	Comment
Melting point above 1500 °F					
Europium	2.88	-----	0.165	1519	----------
Ytterbium	2.78	0.02	.22	1515	----------
Calcium*	2.48	.04	.22	1540	Handleability in air
Manganese	2.44	.65	1.44	2273	----------
Silver	2.18	.15	.687	1761	----------
Copper	1.84	0.09	1.0	1981	----------
Gold	1.58	-----	.725	1965	----------
Cobalt*	1.54	2.04	1.87	2723	Too high a yield
Nickel	1.48	.16	1.875	2647	----------
Thorium*	1.38	.385	.652	3182	Radioactive
Iron	1.3	.16	1.812	2798	----------
Palladium	1.3	-----	1.02	2826	----------
Beryllium*	1.28	.5	2.5	2332	Carcinogenic
Melting point between 1000 and 1500 °F					
Plutonium*	6.11	0.74	0.875	1184	Radioactive
Magnesium	3.01	.24	.375	1202	----------
Aluminum	2.62	.05	.56	1220	----------

*Unlikely candidate; see comment.

TABLE XIV. - ALLOY CANDIDATE COMPLIANT LAYER MATERIALS FOR SCS-6/Ti_3Al + Nb COMPOSITE SYSTEM

Alloy	Coefficient of thermal expansion, α/α^m	Yield stress, σ_y/σ_y^m	Modulus of elasticity, E/E^m	Melting point, °F	Comment
Yellow brass	2.1	0.33	0.875	1710	----------
Ni-Ag cast (20 percent)	2.0	.46	-----	1980	----------
Red brass	1.96	.3	.937	1875	----------
Silicon bronze	1.9	.41	.937	1865	----------
Phosphor bronze	1.88	.37	.937	1920	----------
Stainless steel 321, 347	1.86	.55	-----	2550	----------
Al bronze	1.84	.46	.937	1900	----------
Incoloy 800	1.58	.67	1.77	2475	----------
Incoloy 801*	1.56	1.04	1.88	2475	Too high a yield
Incoloy 802*	↓	.78	1.85	2450	Too high a yield
Durimet T		.65	1.42	----	----------
Monel		.65	1.625	2370	----------
N-155*	1.55	1.08	1.83	2325	Too high a yield
Inconel 690*	1.5	.83	1.9	2450	Too high a yield
Hastelloy-X*	1.54	.96	1.78	2300	Too high a yield

*Unlikely, candidate; see comment.

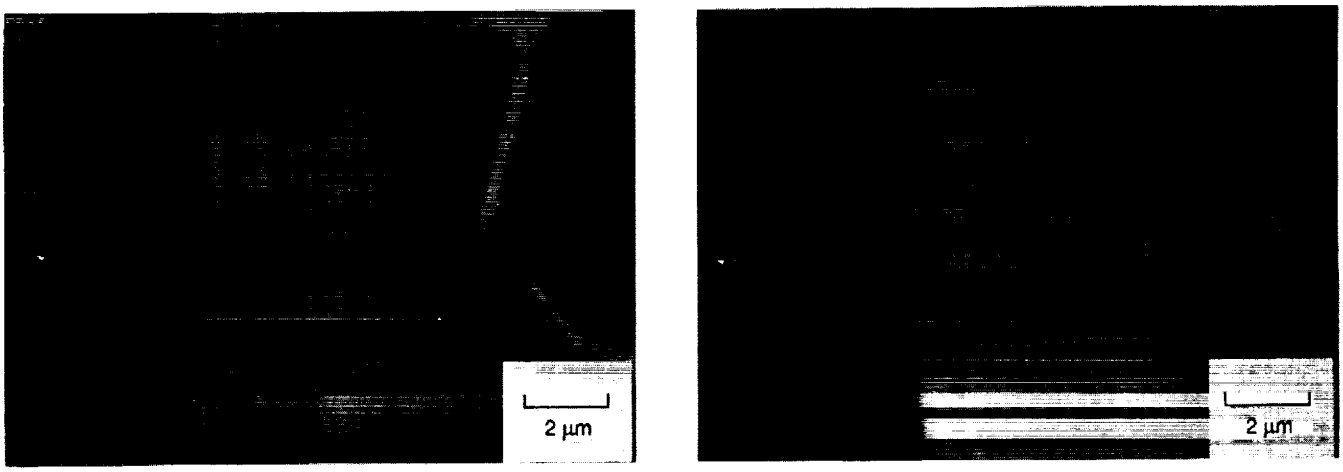

(a) As fabricated.

(b) After 1000 thermal cycles.

Figure 1.—Experimentally observed radial cracking in SIC/TI-24AI-11Nb after fabrication and after an additional 1000 thermal cycles, taken from reference 1.

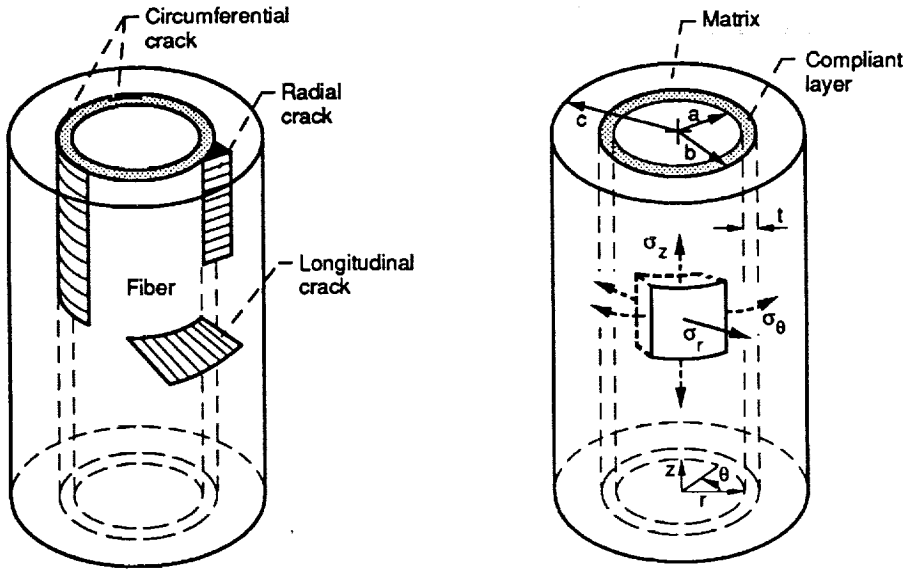

(a) Possible internal crack orientations.

(b) Unit cell and coordinate system.

Figure 2.—Definition of concentric cylinder model and possible internal crack orientations.

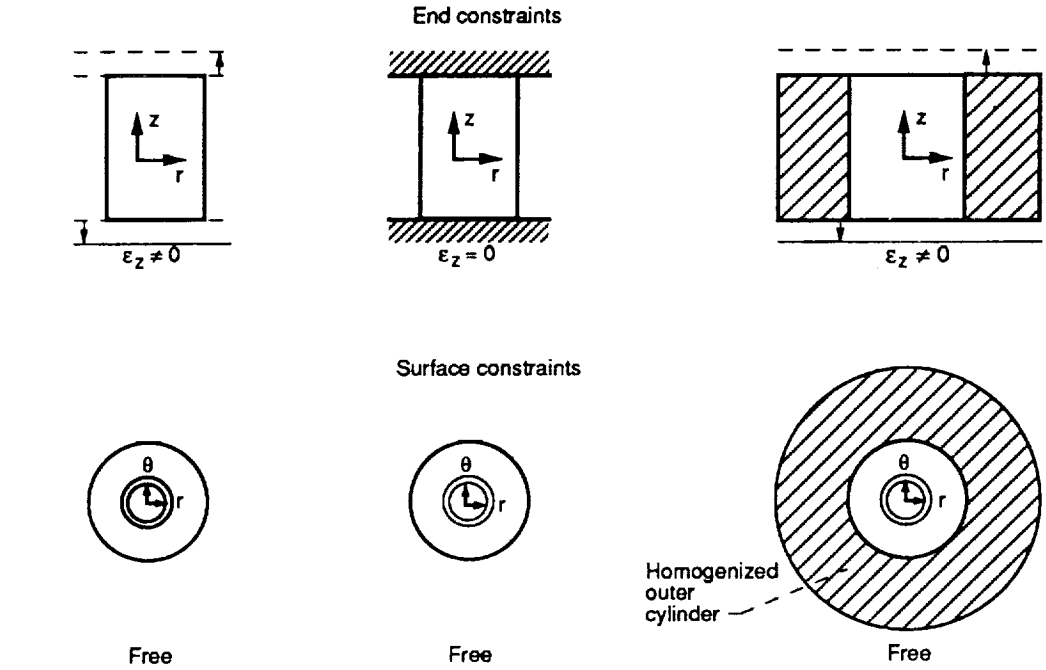

Figure 3.—Various assumed end and surface boundary conditions.

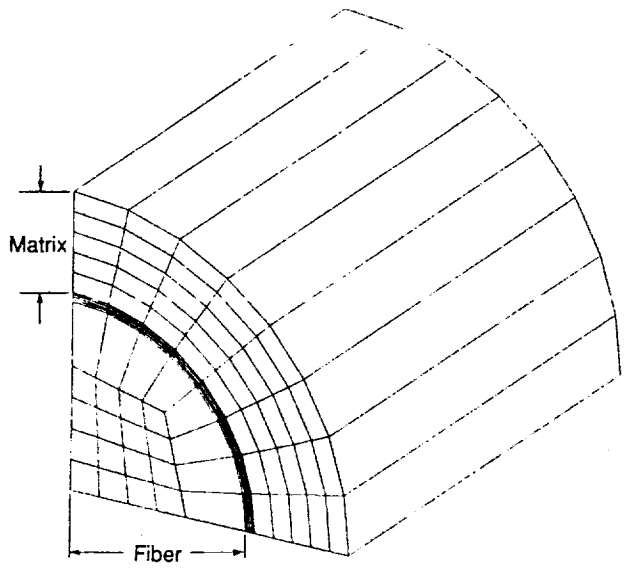

Figure 4.—Finite element concentric cylinder idealization with a compliant layer thickness t/a of 0.05.

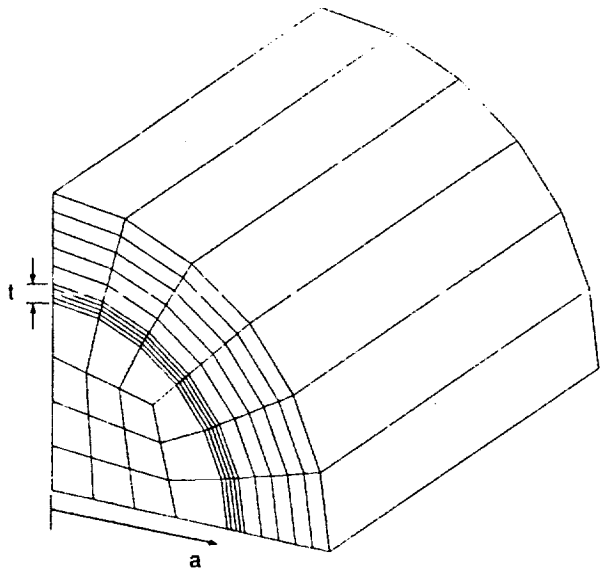

Figure 5.—Finite element concentric cylinder idealization with a compliant layer thickness t/a of 0.10.

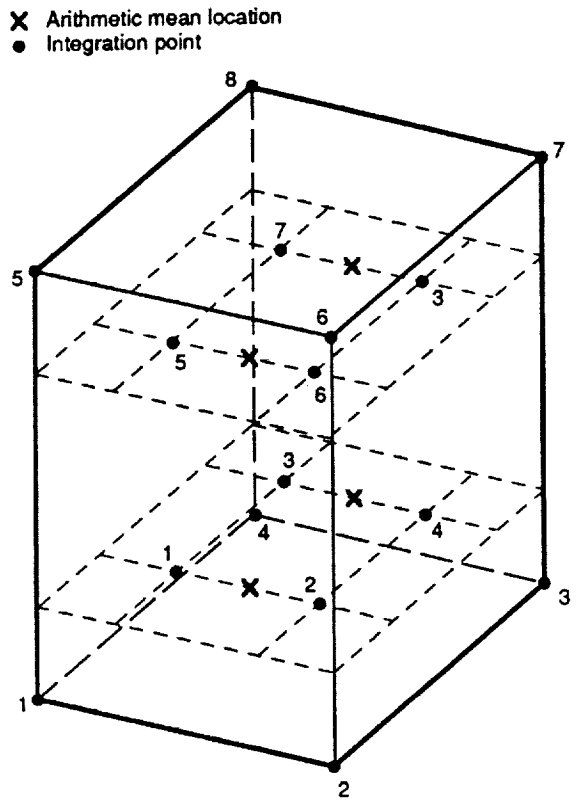

Figure 6.—Illustration of MARC 8-node brick element and 8-point Gauss quadrature integration scheme.

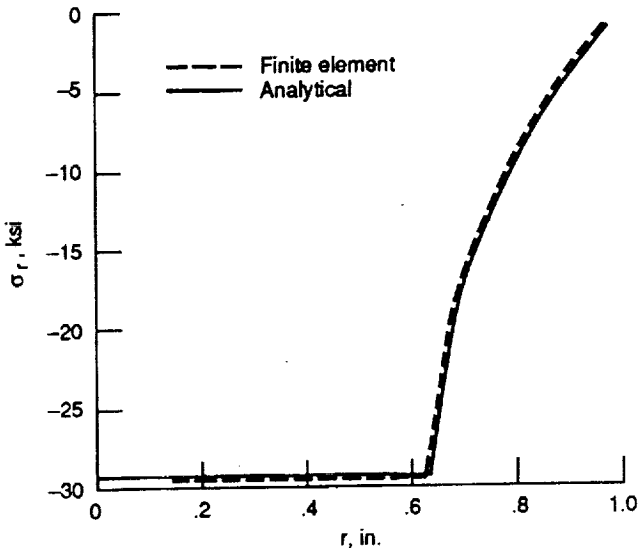

Figure 7.—Comparison between finite element and analytical radial stress versus radial location.

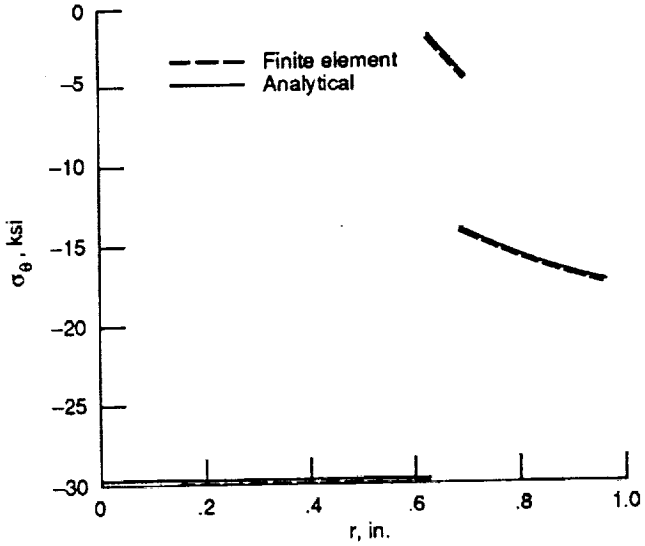

Figure 8.—Comparison between finite element and analytical circumferential stress versus radial location.

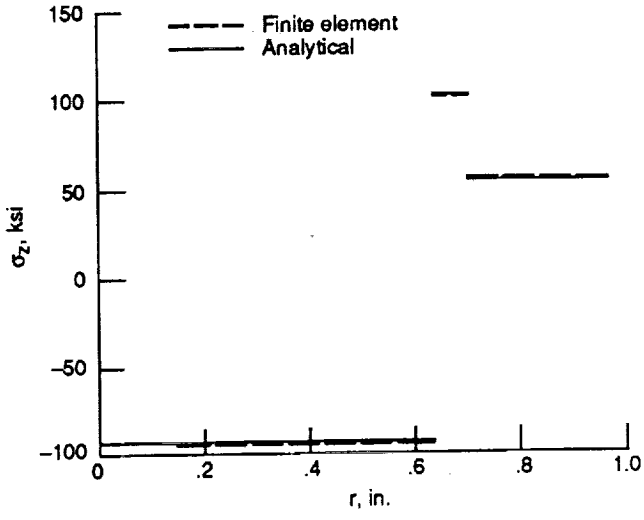

Figure 9.—Comparison between finite element and analytical longitudinal stress versus radial location

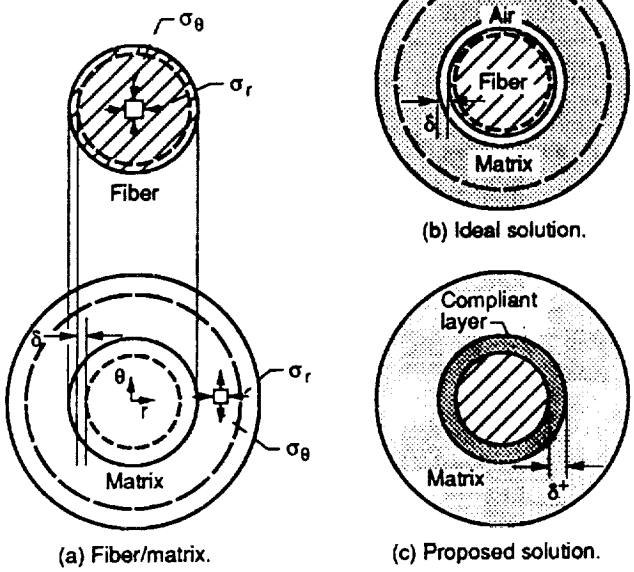

Figure 10.—Description of thermal mismatch problem and compliant/compensating layer solution.

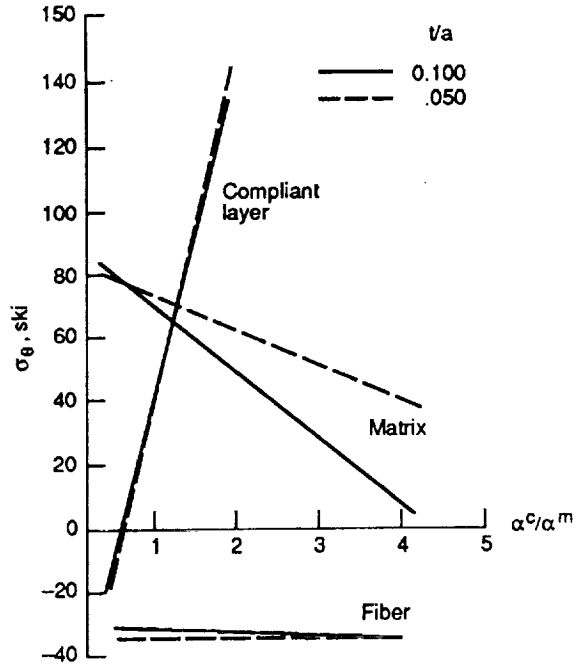

Figure 11.—Effect of varying CTE ratio α^c/α^m and thickness t/a of compliant layer on elastic circumferential stress distribution.

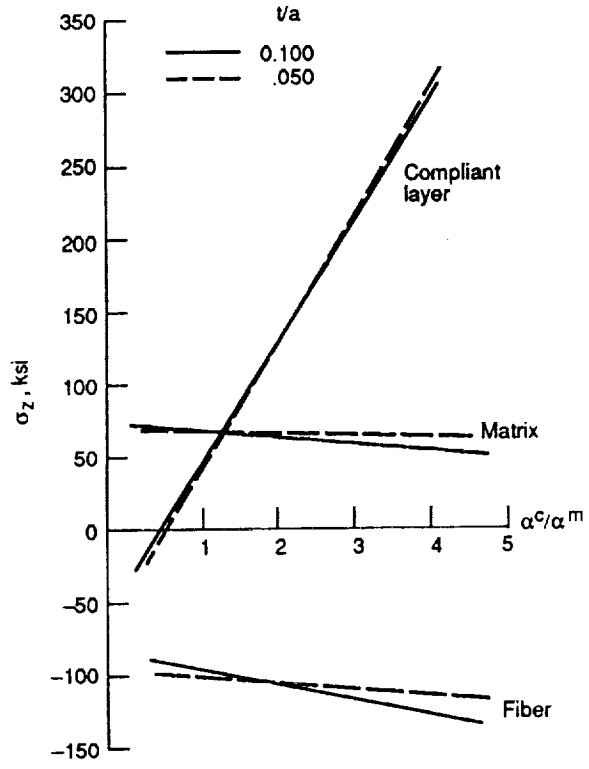

Figure 12.—Effect of varying CTE ratio α^c/α^m and thickness t/a of compliant layer on elastic longitudinal stress distribution.

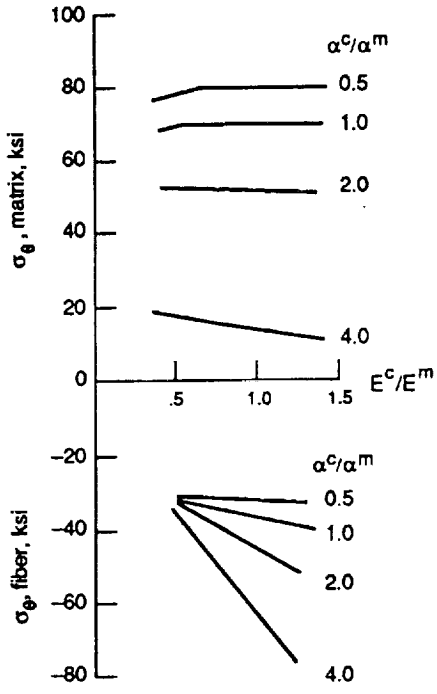

Figure 13.—Effect of varying stiffness of compliant layer (t/a = 0.1) on elastic circumferential stress distribution in fiber and matrix. Inner radius.

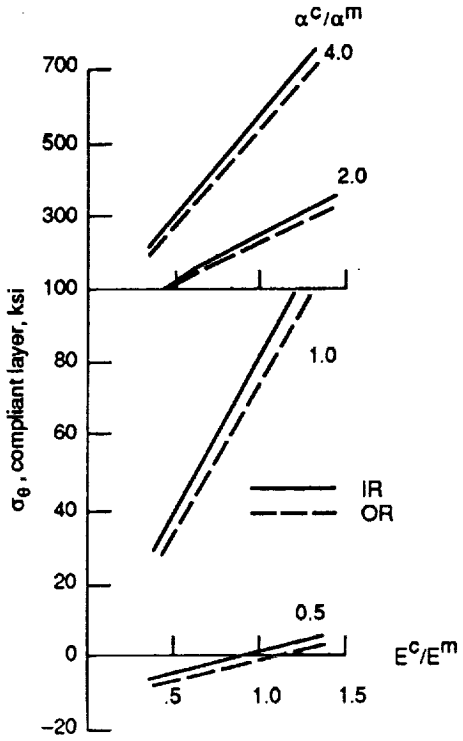

Figure 14.—Effect of varying stiffness of compliant layer on elastic circumferential stress distribution in compliant layer. Inner and outer radii.

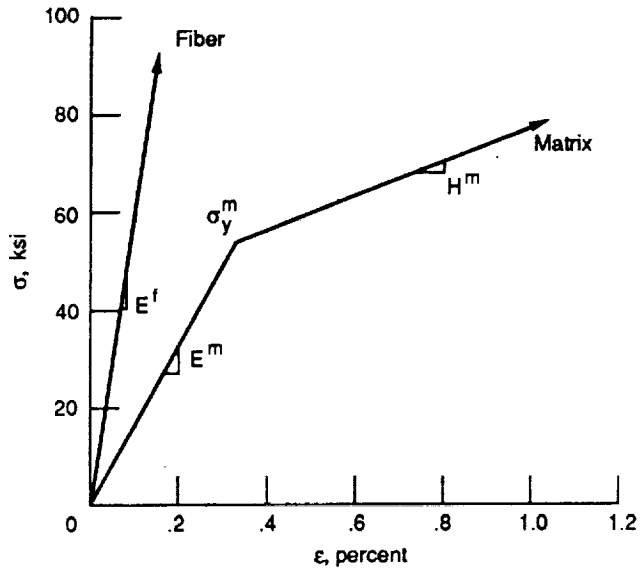

Figure 15.—Stress-strain diagram for SiC fiber and Ti_3 Al matrix at room temperature.

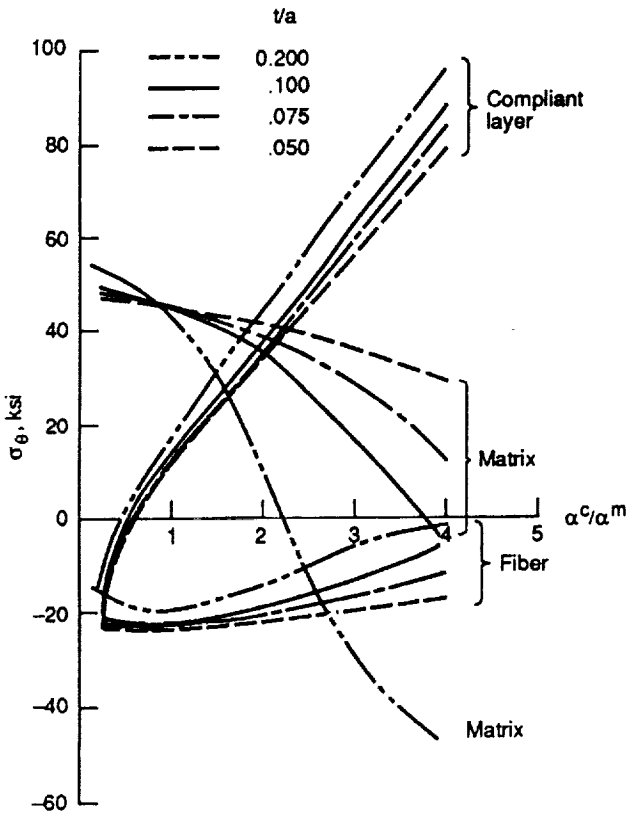

Figure 16.—Effect of varying CTE ratio α^c/α^m and thickness t/a of compliant layer on elastic-plastic circumferential stress distribution.

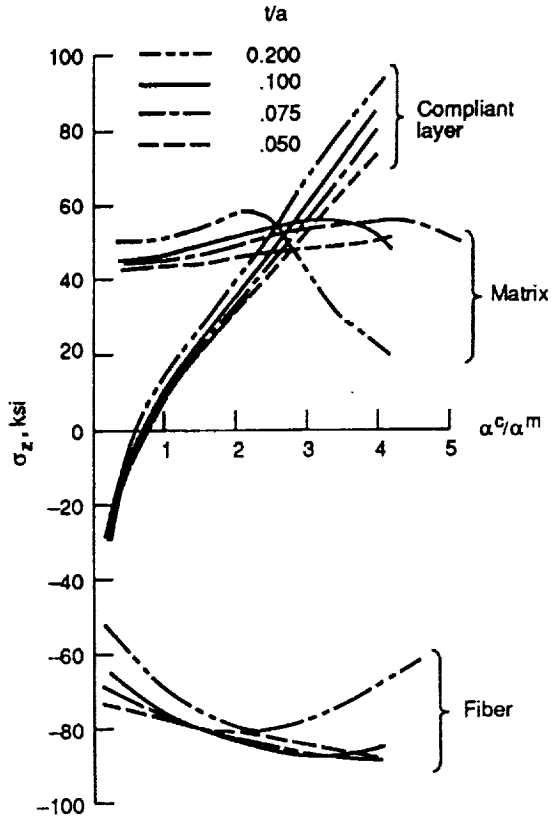

Figure 17.—Effect of varying CTE ratio α^c/α^m and thickness t/a of compliant layer on elastic-plastic longitudinal stress distribution.

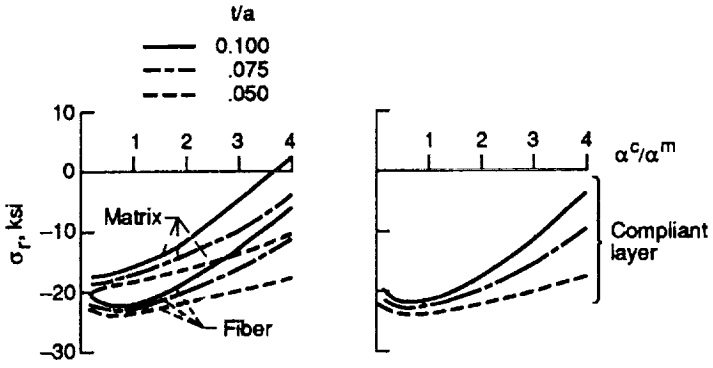

Figure 18.—Effect of varying CTE ratio α^c/α^m and thickness t/a of compliant layer on elastic-plastic radial stress distribution in compliant layer.

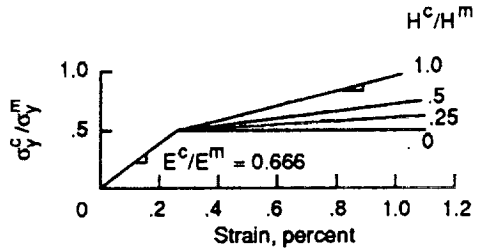

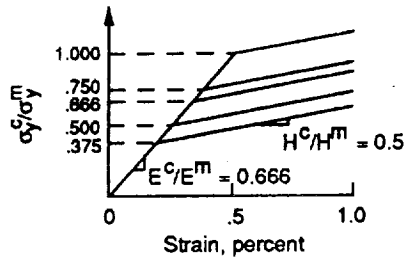

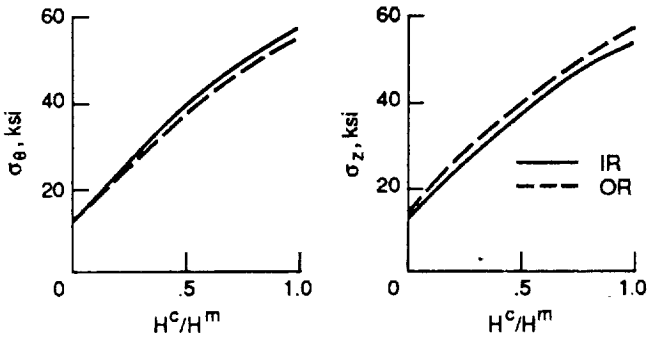

Figure 19.—Effect of varying compliant layer hardening slope H^c/H^m on circumferential and longitudinal (elastic-plastic) stress distribution in compliant layer.

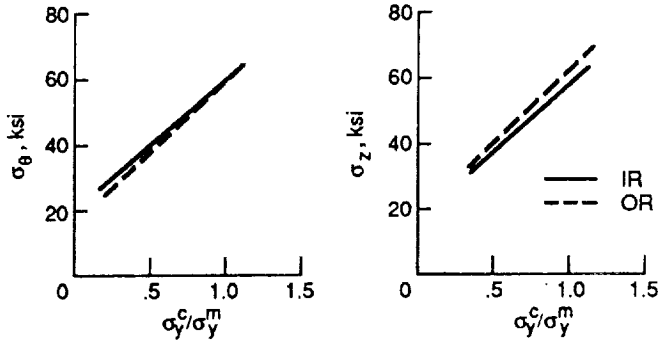

Figure 20.—Effect of varying compliant layer yield point σ_y^c/σ_y^m on circumferential and longitudinal (elastic-plastic) stress distribution in compliant layer.

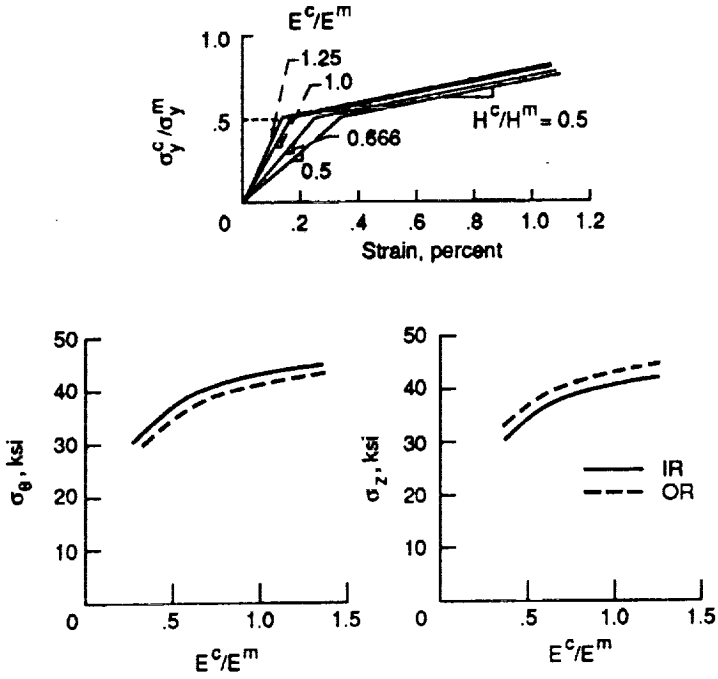

Figure 21.—Effect of varying compliant layer stiffness E^c/E^m on circumferential and longitudinal (elastic-plastic) stress distribution in compliant layer.

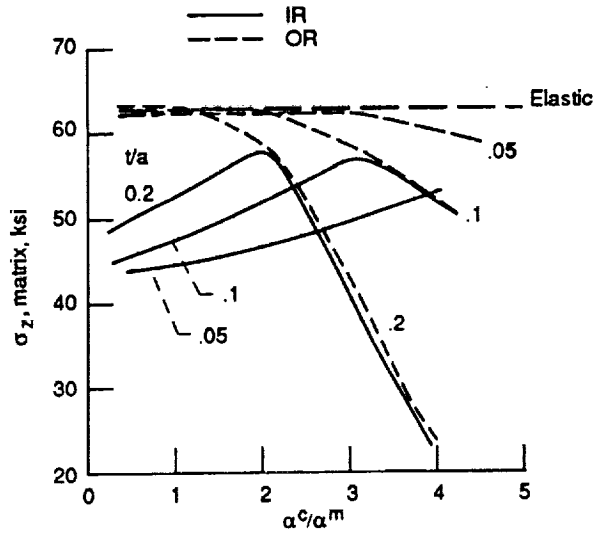

Figure 22.—Longitudinal matrix stress distribution, summarized using inner and outer radial location values, versus normalized CTE ratio α^c/α^m for different compliant layer thicknesses (i.e., t/a = 0.05, 0.1, and 0.2).

NASA
National Aeronautics and Space Administration

Report Documentation Page

1. Report No.	2. Government Accession No.	3. Recipient's Catalog No.
NASA TM-103204		

4. Title and Subtitle

Elastic/Plastic Analyses of Advanced Composites Investigating the Use of the Compliant Layer Concept in Reducing Residual Stresses Resulting From Processing

5. Report Date

September 1990

6. Performing Organization Code

7. Author(s)

Steven M. Arnold, Vinod K. Arya, and Matthew E. Melis

8. Performing Organization Report No.

E-5661

10. Work Unit No.

510-01-01

9. Performing Organization Name and Address

National Aeronautics and Space Administration
Lewis Research Center
Cleveland, Ohio 44135-3191

11. Contract or Grant No.

13. Type of Report and Period Covered

Technical Memorandum

12. Sponsoring Agency Name and Address

National Aeronautics and Space Administration
Washington, D.C. 20546-0001

14. Sponsoring Agency Code

15. Supplementary Notes

Steven M. Arnold, Lewis Research Center; Vinod K. Arya, University of Toledo and National Research Council–NASA Research Associate; Matthew E. Melis, Lewis Research Center.

16. Abstract

High residual stresses within metal and intermetallic matrix composite systems can develop upon cooling from the processing temperature to room temperature due to the coefficient of thermal expansion (CTE) mismatch between the fiber and matrix. As a result, within certain composite systems, radial, circumferential, and/or longitudinal cracks have been observed to form at the fiber-matrix interface region. The compliant layer concept (insertion of a compensating interface material between the fiber and matrix) has been proposed to reduce or eliminate the residual stress buildup during cooling and thus minimize cracking. The present study investigates both elastically and elastic-plastically the viability of the proposed compliant layer concept. A detailed parametric study was conducted utilizing a unit cell model consisting of three concentric cylinders to determine the required character (i.e., thickness and mechanical properties) of the compliant layer as well as its applicability. The unknown compliant layer mechanical properties were expressed as ratios of the corresponding temperature dependent Ti-24Al-11Nb (a/o) matrix properties. The fiber properties taken were those corresponding to SCS-6 (SiC). Results indicate that the compliant layer can be used to reduce, if not eliminate, radial and circumferential residual stresses within the fiber and matrix and therefore also reduce or eliminate the radial cracking. However, with this decrease in in-plane stresses, one obtains an increase in longitudinal stress, thus potentially initiating longitudinal cracking. Guidelines are given for the selection of a specific compliant material, given a perfectly bonded system.

17. Key Words (Suggested by Author(s))	18. Distribution Statement
Residual stress; Thermal mismatch; Elastic; Plastic; Compliant layer; Finite element	Unclassified–Unlimited Subject Category 24

19. Security Classif. (of this report)	20. Security Classif. (of this page)	21. No. of pages	22. Price*
Unclassified	Unclassified	50	A03

*For sale by the National Technical Information Service, Springfield, Virginia 22161